9-14-2018

Growing Signals from the Noise: Challenging Nuclei in Materials DNP

Frédéric A. Perras
Ames Laboratory, fperras@ameslab.gov

Takeshi Kobayashi
Ames Laboratory, takeshi@ameslab.gov

Marek Pruski
Iowa State University and Ames Laboratory, mpruski@iastate.edu

Growing Signals from the Noise: Challenging Nuclei in Materials DNP

Abstract
The polarization of nuclear spins by dynamic nuclear polarization (DNP) has redefined the sensitivity limits of solid-state (SS) NMR spectroscopy. Materials science has been arguably one of the key beneficiaries of the recent remarkable advances of the technique, which included low-temperature magic angle spinning (MAS), modern gyrotrons, and biradical agents for polarization transfer via the cross-effect. In many classes of materials, DNP offers the capability of selectively sensitizing progressively smaller surface and interfacial regions of materials and eliciting responses from previously undetectable nuclei, with no detrimental effect on resolution. We review the most recent applications of DNP-enhanced SSNMR to materials, focusing specifically on measurements that pose insurmountable challenges to conventional SSNMR, including the detection of 15N, 17O, 25Mg, 35Cl, 43Ca, 79Br, 89Y, 119Sn, and 195Pt by one-dimensional MAS methods, ultrawideline NMR, as well as two-dimensional homo- and heteronuclear correlation spectroscopy.

Keywords
solid-state NMR, dynamic nuclear polarization (DNP), sensitivity enhancement, homonuclear correlation spectroscopy, heteronuclear correlation spectroscopy, wideline NMR, unreceptive nuclei

Disciplines
Condensed Matter Physics | Nanoscience and Nanotechnology

Growing Signals from the Noise: Challenging Nuclei in Materials DNP

Frédéric A. Perras[1], Takeshi Kobayashi[1] & Marek Pruski[1,2]

[1] *U.S. DOE Ames Laboratory, Ames, IA, USA*
[2] *Department of Chemistry, Iowa State University, Ames, IA, USA*

The polarization of nuclear spins by dynamic nuclear polarization (DNP) has redefined the sensitivity limits of solid-state (SS) NMR spectroscopy. Materials science has been arguably one of the key beneficiaries of the recent remarkable advances of the technique, which included low-temperature magic angle spinning (MAS), modern gyrotrons, and biradical agents for polarization transfer via the cross-effect. In many classes of materials, DNP offers the capability of selectively sensitizing progressively smaller surface and interfacial regions of materials and eliciting responses from previously undetectable nuclei, with no detrimental effect on resolution. We review the most recent applications of DNP-enhanced SSNMR to materials, focusing specifically on measurements that pose insurmountable challenges to conventional SSNMR, including the detection of ^{15}N, ^{17}O, ^{25}Mg, ^{35}Cl, ^{43}Ca, ^{79}Br, ^{89}Y, ^{119}Sn, and ^{195}Pt by one-dimensional MAS methods, ultrawideline NMR, as well as two-dimensional homo- and heteronuclear correlation spectroscopy.

Keywords: solid-state NMR, dynamic nuclear polarization (DNP), sensitivity enhancement, homonuclear correlation spectroscopy, heteronuclear correlation spectroscopy, wideline NMR, unreceptive nuclei

How to cite this article:
eMagRes, 2018, Vol 7: 35–50. DOI 10.1002/9780470034590.emrstm1556

Introduction

Dynamic nuclear polarization (DNP) has revolutionized various areas of solid-state (SS) NMR spectroscopy. Materials science has been arguably one of the key beneficiaries of the recent remarkable advancement of the technique. Indeed, in many classes of materials, DNP offers sensitivity enhancements of two orders of magnitude, and often even larger savings of experimental time. Importantly, these gains in sensitivity are rarely accompanied by lower resolution since linewidths are typically controlled by the inhomogeneous effects due to material's heterogeneity and the effects of paramagnetic broadening are usually very minor in comparison. Finally, the recently developed dynamic nuclear polarization surface-enhanced NMR spectroscopy (DNP SENS) has endowed researchers with the capability of selectively sensitizing progressively smaller surface and interfacial regions of materials and eliciting responses from previously undetectable nuclei. As a result, DNP has already helped advance structural studies of catalysts, mesoporous solids, nanoparticles, glasses, polymers, and pharmaceuticals, and yet further progress is underway with new developments in ultralow-temperature, and fast, magic-angle spinning (MAS) technologies, microwave technology, the development of new polarizing agents, and theory.

In this article, we will review the most recent applications of DNP-enhanced SSNMR to materials, focusing specifically on two groups of measurements that pose insurmountable challenges to conventional SSNMR, at least without isotope enrichment: (i) the detection of important yet insensitive nuclei, such as ^{15}N, ^{17}O, ^{25}Mg, ^{35}Cl, ^{43}Ca, ^{79}Br, ^{89}Y, ^{119}Sn, and ^{195}Pt, which is mostly, but not exclusively, performed using one-dimensional (1D) schemes and (ii) the acquisition of two-dimensional (2D) correlation spectra involving dilute nuclei, such as ^{13}C and ^{29}Si. Our review includes primarily the applications reported following the resurgence of DNP in the past 20 years, subsequent to the development of low-temperature MAS,[1] modern gyrotrons,[2] and biradical agents for polarization transfer via the cross-effect.[3–6] Earlier applications of the technique, which relied primarily on the solid effect, were comprehensively reviewed by Wind.[7] Similarly, most of the experimental parameters have been omitted for the sake of brevity. We do, however, include information about the observed enhancements, as they define the technique's key impact on SSNMR spectroscopy. In most cases, the enhancements have been reported as the ratio of signal intensities observed with and without microwave irradiation ($\varepsilon_{on/off}$). These are not equivalent to the absolute sensitivity gains, which depend on a number of other parameters, including longitudinal relaxation, polarization buildup time, and quenching effects[8,9] and are rarely reported with high precision.

Detection of Challenging Nuclei

^{17}O

Oxygen is ubiquitous in nature and plays an important role in materials science, yet applied SSNMR studies of ^{17}O, the only NMR active isotope of oxygen, are very rare. This may appear surprising given the fact that ^{17}O has a very wide chemical shift range of approximately 1200 ppm, and, as a result, ^{17}O SSNMR spectra are generally very informative. Although ^{17}O is a quadrupolar nucleus ($I = 5/2$), it has one of the smallest quadrupole moments of any naturally occurring nuclide at −25.58 mb, and thus the linewidths are often quite manageable, allowing for the resolution of large numbers of resonances in solids, particularly at high magnetic fields.[10–13] This quadrupolar broadening is also valuable as it allows for the study of dynamics,[14] and additionally enables the determination of precise local and long-range structural information in a way that is not possible for spin-1/2 nuclei.[15,16] Notwithstanding these favorable features, the main hurdle that has limited the application of ^{17}O SSNMR is its extremely low natural abundance of 0.038%. Although natural abundance ^{17}O spectra can be, in principle, acquired by conventional SSNMR, using high magnetic fields, large sample quantities, and pulse sequences for enhancing the population difference across the central transition,[17] such experiments usually require prohibitively long data acquisition times. Isotopic enrichment, on the other hand, has limited applications due to synthetic challenges and the lack of commercially available sources of ^{17}O, which are limited to costly $^{17}O_2$ gas, $H_2{}^{17}O$, and a few small organics.

^{17}O is thus an exemplary nuclide for demonstrating the transformative force of DNP. The technique is theoretically capable of yielding sensitivity enhancements of up to $\gamma_e/\gamma_{^{17}O} \approx 4855$; if achieved, such enhancements would nearly double that obtainable by 100% ^{17}O enrichment. This opportunity was recognized early on, and the first ^{17}O SSNMR experiments performed on a noncubic solid, by Niebuhr *et al.*, were performed using DNP enhancement.[18] This seminal experiment was performed on a single crystal of ruby, using endogenous Cr^{3+} as the polarization source, at a magnetic field strength of 1 T and temperature of 1.9 K. No enhancement factors were quoted, but an ^{27}Al DNP enhancement factor of 360 was reported on the same material. Further advancements in ^{17}O DNP did not, however, take place until the development of high-field DNP instrumentation.

Michaelis *et al.*[19] were the first to apply modern high-field DNP to the ^{17}O nuclide. Using an indirect DNP approach, where electrons' polarization is transferred via a high-γ nuclide such as proton, they obtained a DNP enhancement, $\varepsilon_{on/off}$, of 80 on a ^{17}O-enriched water sample at a magnetic field strength of 5 T and a temperature of 85 K. Although this was not extensively discussed in their paper, they also managed to detect the ^{17}O SSNMR signal in a natural abundance sample of 'DNP juice' (60/30/10% v/v d_8-glycerol/D_2O/H_2O with 20 mM TOTAPOL[20]) using the quadrupolar Carr-Purcell Meiboom-Gill (QCPMG) pulse sequence.[21] The earliest application of natural abundance ^{17}O DNP to materials was demonstrated by Blanc *et al.*[22] who again used indirect DNP, in combination with QCPMG, to acquire ^{17}O MAS spectra of $Ca(OH)_2$ and $Mg(OH)_2$ samples. DNP enabled them to perform these difficult experiments in a mere 10 min, thus facilitating the acquisition of a 2D $^{17}O\{^1H\}$ heteronuclear correlation (HETCOR) spectrum. In the same study, the application of direct ^{17}O DNP to ^{17}O-enriched and natural abundance MgO nanoparticles was reported. A sizeable DNP enhancement $\varepsilon_{on/off} = 43$ was achieved using a 20 mM solution of bTbK[4] in 1,1,2,2-tetrachloroethane, which could be further quadrupled with the use of a double-frequency sweep (DFS) pulse[23,24] to transfer hyperpolarization from the satellite transitions to the observed central transition of ^{17}O. Notably, this study enabled the enhancement and detection of an oxygen site at the MgO surface.

Perras *et al.*[25] later built on the work of Blanc and performed the first ^{17}O DNP SENS experiments on a mesoporous silica nanoparticle (MSN) sample. The success of this study rested on the use of PRESTO (phase-shifted recoupling effects a smooth transfer of polarization),[26] as opposed to CP, for the transfer of ^1H hyperpolarization to ^{17}O. Given that the application of a spin locking pulse can lead to large losses in magnetization for quadrupolar nuclei, the PRESTO sequence, which is considerably simpler to apply at the ^{17}O frequency as it necessitates only the application of a spin echo, was shown to lead to ∼5 times greater sensitivity.[25] Notwithstanding the detection of dilute silanol species on an MSN sample, PRESTO further enabled the acquisition of ^1H–^{17}O dipolar coupling data showing the presence of both hydrogen-bonded and mobile silanols. In a subsequent study, the same authors resolved these two silanol species and monitored the dehydroxylation of the hydrogen-bonded site upon thermal treatment (Figure 1a) by means of $^{17}O\{^1H\}$ HETCOR experiments.[27] Lastly, they used indirect DNP to perform $^{17}O\{^1H\}$ windowed proton-detected local field (wPDLF) experiments[28] on a series of different oxide materials.[29] The wPDLF experiment, which is insensitive to chemical shift anisotropy (CSA) and radio frequency (RF) field maladjustments and inhomogeneity, enabled the measurement of O–H bond lengths with subpicometer precision and provided confirmation of the longstanding assumption that the Brønsted acidity of surface sites is correlated to the hydroxyl group's O–H bond length (Figure 1b–d). Similar experiments performed on samples impregnated with pyridine were also able to conclusively show the formation of intermolecular hydrogen bonds at the silica surface, while the more Lewis-basic alumina surfaces form no such interactions with pyridine.[30]

Although significant insights into material surfaces could be obtained using indirect ^{17}O DNP, this approach is inherently limited to oxygens in the vicinity of hydrogen; in practice, only hydroxyls can be reliably detected. In order to tackle structural problems in a wider range of materials, direct ^{17}O DNP spectroscopy needed to be developed. Following the abovementioned work by Blanc *et al.*,[22] Michaelis *et al.*[31] discovered that higher ^{17}O DNP enhancements could be obtained when using a narrow-line trityl radical as a polarization source. These authors reported enhancement factors ($\varepsilon_{on/off}$) of 115 for water, ≥80 for urea, and ≫100 for phenol at a magnetic field of 5 T and a temperature of 85 K. Hope *et al.*[32] subsequently applied ^{17}O direct DNP to probe the surface structure of ceria nanoparticles. Importantly, they were able to show that ^{17}O

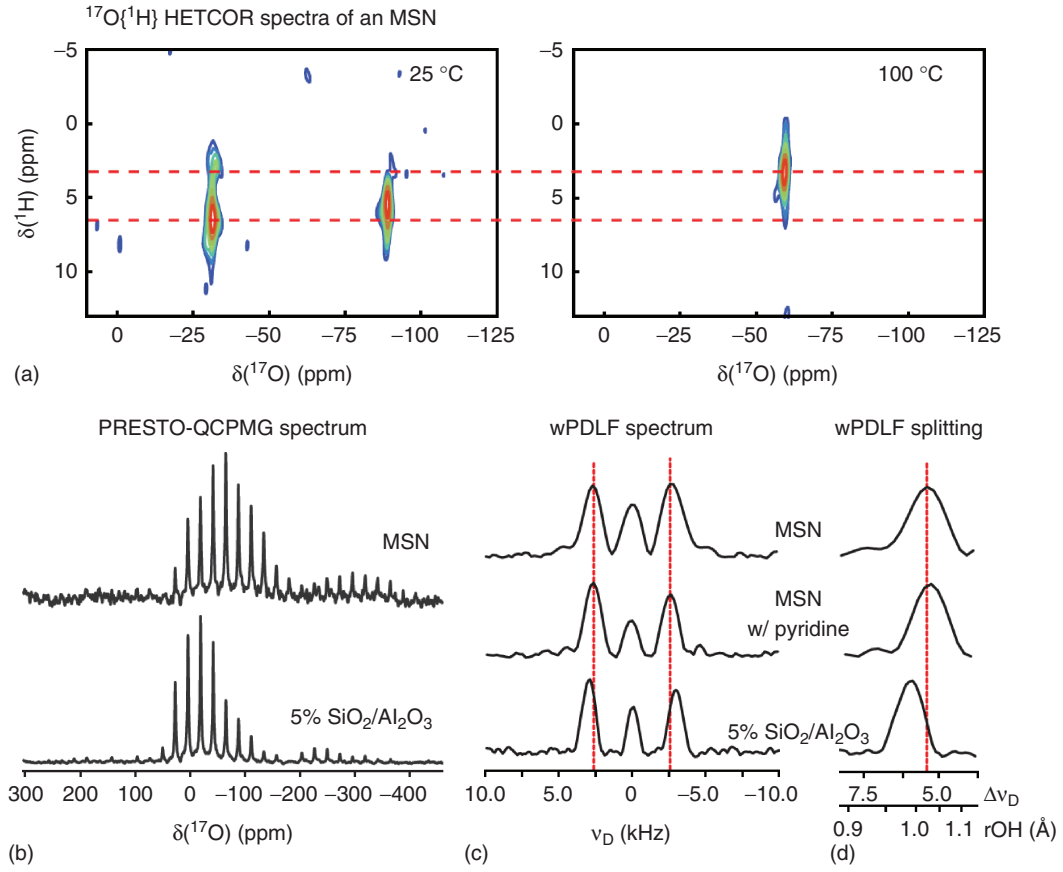

Figure 1. Natural abundance ^{17}O NMR data of the surfaces of oxide materials acquired with the use of DNP. (a) $^{17}O\{^1H\}$ PRESTO-QCPMG HETCOR spectra of MSNs thermally treated at 25 and 100 °C showing the resolution of two types of silanols along the ^{1}H dimension, the hydrogen-bonded silanols being removed by thermal treatment . (b) 1D PRESTO-QCPMG spectra of hydroxyl moieties in silica and alumina materials. (c,d) $^{17}O\{^1H\}$ wPDLF spectra of silica and alumina materials showing the changes in bond lengths that are associated with Brønsted acidity. The addition of pyridine to the MSN also lengthens the O–H bond and provides evidence of the formation of intermolecular hydrogen bonding interactions at the surface. ((a) Reprinted with permission from F. A. Perras, U. Chaudhary, I.I. Slowing, and M. Pruski, J. Phys. Chem. C, 2016, 120, 11535. Copyright 2016 American Chemical Society. (b–d) Reproduced with permission from Ref. 29. © John Wiley and Sons, 2017)

direct DNP experiments of materials are surface selective, showing far faster signal buildup rates for the surface and subsurface sites than the bulk sites (Figure 2). The buildup rates and enhancement factors for the three first layers, however, did not correlate with their distance from the surface because the buildup rates were limited by the T_1 relaxation of ^{17}O, as is common for most DNP experiments. The studies by Hope *et al.* were performed at a magnetic field of 14.1 T, which showed strong promise for the application of ^{17}O DNP at even higher magnetic fields where the spectral resolution would be considerably improved. Indeed, Blanc *et al.* recently carried out ^{17}O indirect DNP experiments at an ultrahigh magnetic field of 18.8 T,[33,34] thereby demonstrating the possibility of using Overhauser effect-based DNP transfer for the measurement of highly resolved ^{17}O spectra in natural abundance materials.

^{15}N

Nitrogen's prominence in many areas of materials science rivals that of oxygen, and so do the ways in which its NMR-active nuclei, ^{14}N and ^{15}N, pose spectroscopic challenges. Both these nuclei have low gyromagnetic ratios (γ), smaller than that of ^{1}H by factors of roughly 10 (^{15}N) and 14 (^{14}N), but they differ significantly in terms of natural abundance and their spin quantum number, I. The ^{14}N isotope is highly abundant (99.6%) but is an integer spin quadrupolar nuclide ($I = 1$). The resulting first-order quadrupolar broadening renders MAS ineffective and necessitates the use of complex wideline or indirect detection schemes, but even such methods can rarely provide practical site resolution in complex structures. For this reason, there have been concerted efforts to enable detection of the ^{15}N nuclide, for which $I = 1/2$. In contrast to ^{14}N, ^{15}N can thus yield highly resolved MAS spectra, but its very low natural abundance (0.4%) poses a sensitivity problem. To alleviate this problem, researchers have developed the indirectly detected heteronuclear correlation (idHETCOR) technique, which allows for the acquisition of $^1H\{^{15}N\}$ spectra of naturally abundant bulk materials, such as peptides and pharmaceuticals.[35] Nevertheless, natural abundance ^{15}N studies of surface and interfacial regions have generally remained beyond the detection limits of SSNMR. Modern DNP-enhanced SSNMR has quickly emerged as a method of choice for such studies,

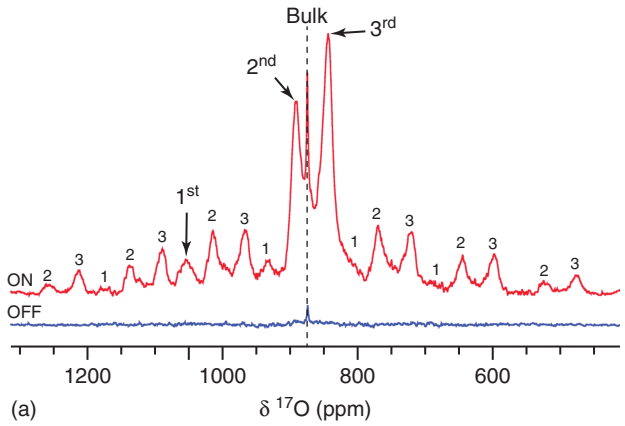

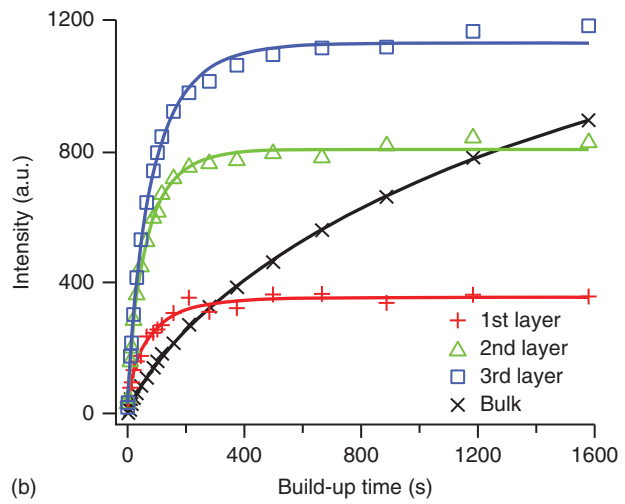

Figure 2. (a) ^{17}O direct DNP-enhanced MAS spectrum of a ^{17}O-enriched CeO_2 sample, with clearly identifiable resonances from the first three layers of the material. The spectrum acquired with microwave irradiation 'off' is shown at the bottom. (b) ^{17}O saturation recovery curves for the different oxygen environments of the material, which clearly demonstrate the faster buildup of the surface sites. (Source: Hope *et al.*,[32] http://pubs.rsc.org/-/content/articlehtml/2017/cc/c6cc10145c. Licensed under CC BY 3.0)

enabling the acquisition of 1D and 2D natural abundance ^{15}N spectra of porous materials, such as mesoporous silica materials,[36–42] metal-organic frameworks (MOFs),[42–46] or organic porous polymers.[47] ^{15}N DNP has also been applied to studies of nonporous materials, for which providing access to the polarization source is an ongoing challenge;[48–51] in some cases in combination with isotopic enrichment.[52–55] In the subsequent paragraphs we will highlight a few of these studies.

The first application of modern ^{15}N DNP-enhanced SSNMR in materials science was reported in 2012 by Zagdoun *et al.*,[36] who tracked the stepwise postfunctionalization of a propyl azide moiety (PrN_3) attached to the surface of mesoporous silica, and the subsequent formation of imidazolium-containing materials (PrIm) using ^{15}N and ^{13}C NMR (see Figure 3). The ^{15}N NMR spectra unambiguously identified the chemical structures of the functional groups at each reaction step, which was not possible with the use of ^{13}C NMR spectroscopy alone. Gutmann *et al.*[38] later used a similar approach to study the interactions between surface amine functionalities and a dirhodium catalyst. They observed that the immobilization of $Rh_2(CH_3COO)_4$ led to a decrease in the intensity of the ^{15}N NMR signal assigned to amine functionalities and a concomitant appearance of new signals attributed to the interactions between the dirhodium catalyst and the amine moiety.

DNP has also been used to enhance the ^{15}N SSNMR signals in natural abundance MOFs.[43,44] In particular, the technique was used to interrogate the host–guest interactions between Pt^{2+} and NH_2 groups in a UiO-66-NH_2 MOF (Figure 4).[44] In addition to the ^{15}N peaks at −315 and −242 ppm from the $-NH_2$ and $-NH_3^+Cl$ moieties in UiO-66-NH_2, the Pt-containing sample showed a distinct peak at −388 ppm whose intensity increased linearly with the metal content. DNP-enhanced ^{15}N SSNMR thus provided credible evidence of chemical bonding between the Pt^{2+} and the $-NH_2$ moieties of the MOF. The use of a nonprotonated DNP solvent, DMSO-d_6, yielded a background-free 2D ^{15}N{^{1}H} HETCOR spectrum with well-resolved cross-peaks from $-NH_2$ and $-NH_2\cdots Pt^{2+}$ moieties in Pt/UiO-66-NH_2. This HETCOR experiment enabled the distinction of a ∼1 ppm ^{1}H chemical shift increase upon the coordination of the amine group to Pt^{2+} (Figure 4b).[42]

As previously mentioned, DNP-enhanced ^{15}N SSNMR spectroscopy has also been applied to nonporous materials. For instance, DNP-enhanced ^{15}N SSNMR of nitridated fibrous silica, which holds promise in applications for CO_2 capture and as a solid base catalyst, helped to determine that the catalytic deactivation of the material at higher nitridation temperatures was the result of a decrease in the number of Si-NH_2 sites, despite the concomitant increase of the overall nitrogen content.[53] In another study, ^{15}N DNP-enhanced SSNMR spectroscopy was used to monitor the dehydrogenation process of ammonia borane, a promising medium for hydrogen storage. The use of DNP, in combination with conventional ^{11}B multiple-quantum (MQ) MAS, ^{1}H{^{15}N} idHETCOR, and density functional theory (DFT) calculations of the magnetic shielding tensors, revealed that the oligomerization of ammonia borane proceeds in a 'head-to-tail' manner, ultimately leading to the formation of hexagonal boron nitride via a dehydrocyclization reaction, bypassing the formation of polyiminoborane.[48] At present, DNP investigations of nonporous materials or samples with very small pores, such as MOFs, rely on ^{1}H–^{1}H spin diffusion to transport the hyperpolarization into the bulk before being transferred to the nuclei of interest, ^{15}N in this case, by cross-polarization (CP).

^{119}Sn

Given its high gyromagnetic ratio and I value of 1/2, ^{119}Sn may not seem a particularly challenging nucleus; however, the acquisition of ^{119}Sn SSNMR spectra in many materials of interest has been exceedingly difficult due to the large chemical shift distributions and the low loadings typical of tin. As a result, ^{119}Sn SSNMR spectroscopy of materials has greatly benefitted from the development of DNP, which has enabled the acquisition of SSNMR spectra that were previously out of reach. The first application of DNP to ^{119}Sn SSNMR was in the elucidation of the core–shell structure of Sn/SnO_x colloidal nanoparticles.[56] ^{119}Sn DNP SENS measurements, which feature solely the signals from the particle surface due

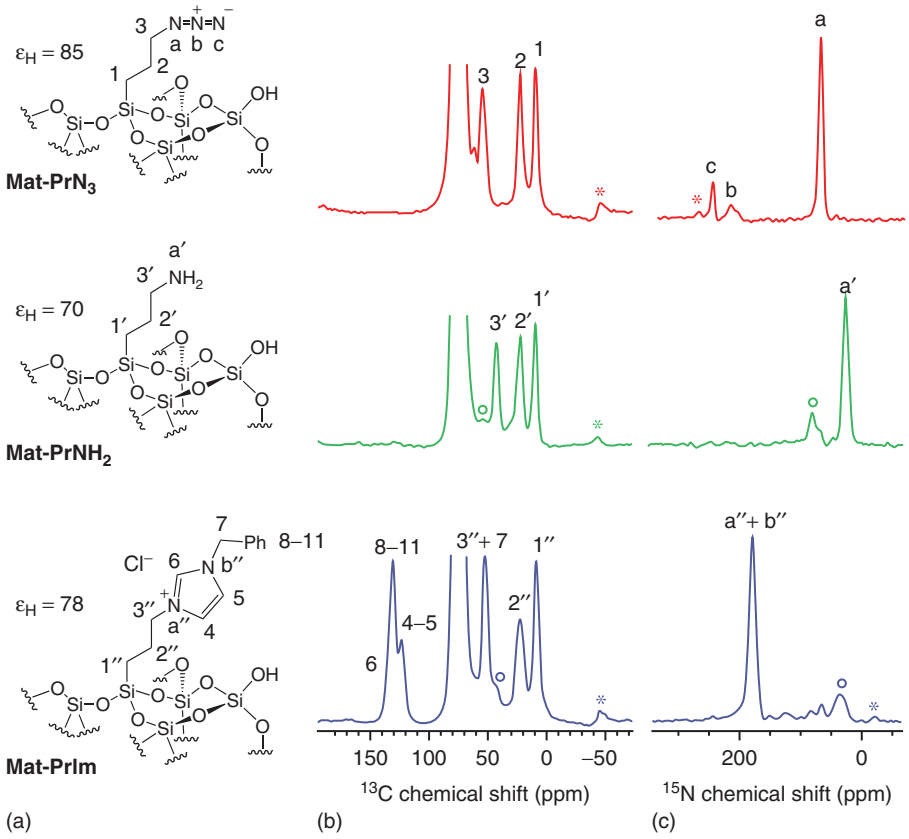

Figure 3. DNP-enhanced $^{13}C\{^1H\}$ (b) and $^{15}N\{^1H\}$ (c) CPMAS spectra of the functionalized hybrid organic–inorganic silica materials depicted in (a). (Reprinted with permission from A. Zagdoun, G. Casano, O. Ouari, G. Lapadula, A. J. Rossini, M. Lelli, M. Baffert, D. Gajan, L. Veyre, W. E. Maas, M. Rosay, R. T. Weber, C. Thieuleux, C. Copéret, A. Lesage, P. Tordo and L. Emsley, J. Am. Chem. Soc., 2012, 134, 2284. Copyright 2012 American Chemical Society)

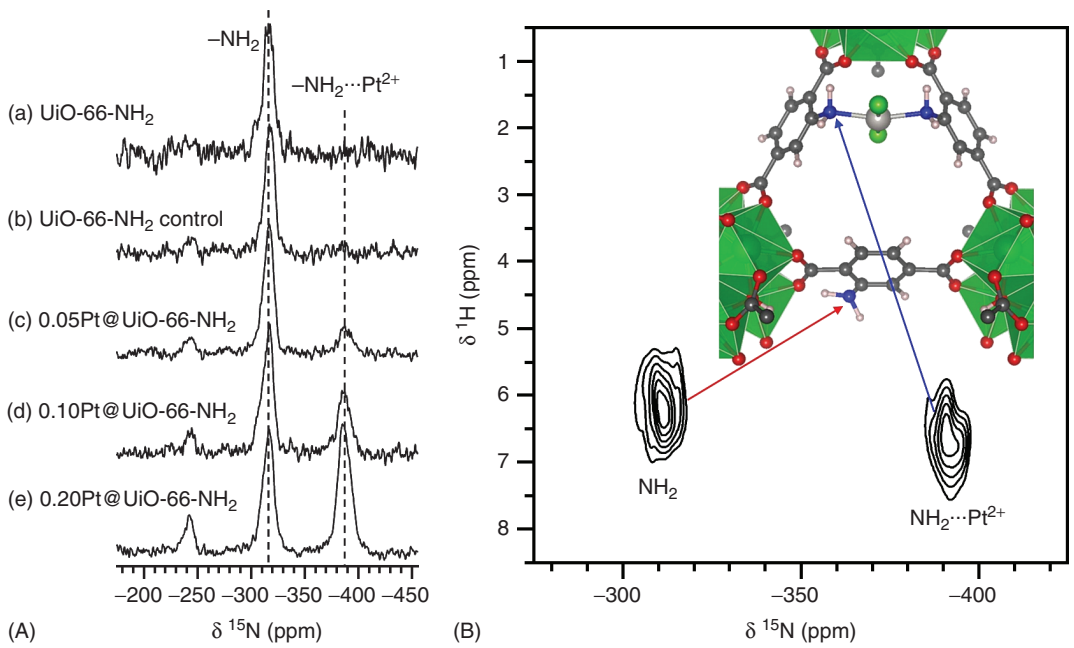

Figure 4. DNP-enhanced $^{15}N\{^1H\}$ CPMAS (A) and 2D $^{15}N\{^1H\}$ HETCOR spectra of Pt^{2+}/UiO-66-NH_2 (B). ((A) Reproduced with permission from Ref. 44. © John Wiley and Sons, 2014. (B) Reproduced with permission from Ref. 42. © Elsevier, 2017)

to a lack of ^{1}H spins in the bulk, were able to show that the outer shell of the nanoparticles was composed exclusively of SnO_2, while the SnO and Sn phases, detected by Mössbauer spectroscopy, must be located deeper inside the particle. ^{119}Sn DNP-enhanced SSNMR was also applied to the characterization of Sn-containing zeolites (Sn-BEA[57–59] and Sn-CHA[60]), which usually have tin loadings of only a few percent; these low loadings typically prevent ^{119}Sn detection in the absence of DNP and isotope enrichment. Such ^{119}Sn DNP NMR spectra have been able to yield qualitative information regarding the coordination number of Sn and whether the site is coordinatively open or closed. The CSA parameters extracted using a magic-angle-turning (MAT) experiment[61] were also shown to aid in the assignment of certain resonances to specific sites within the crystal structure, potentially leading to site-specific explanations for the catalytic performance of different zeolites.[59] Importantly, it was revealed that typical nitroxide polarizing agents can coordinate to Sn sites within zeolites,[57] and thus larger, or dendritic,[62] polarizing agents that cannot access the Sn sites should be used. Lastly, ^{119}Sn DNP SENS has been performed on silica-grafted organotin complexes in which the Sn loading was far too low to be detected without DNP.[63] These measurements were able to resolve the ^{119}Sn signals from mono- and bipodal Sn sites on silica and were used to suggest that bipodal complexes are formed by the reorganization of Q^2 sites, rather than vicinal Q^3 sites (where n in Q^n represents the number of next nearest neighbors that are Si).

Low-γ Nuclei

Given the fact that the theoretical gain in sensitivity from the application of DNP corresponds to the ratio of the γ value of the electron and the nucleus, one of the areas that shows the greatest promise for applications of DNP is SSNMR spectroscopy of low-γ nuclei. The working definition of what constitutes a low-γ nuclide is any nuclide that has a γ value which is smaller than that of ^{15}N (i.e., resonance frequency <40 MHz at a field of 9.4 T), as the NMR spectroscopy of these nuclides typically requires the use of additional specialized hardware.[64,65] These isotopes are very rarely studied not only due to hardware limitations but also due to their unfavorable relaxation properties, low signal amplitudes, and poor CP dynamics, requiring the use of long, high-RF, spin-locking pulses. Nevertheless, the possibilities afforded by DNP have been recognized and, to date, four low-γ isotopes (^{14}N, ^{25}Mg, ^{43}Ca, and ^{89}Y) have been investigated with the use of DNP. Some of the results obtained for materials will be discussed here, while applications of DNP to ^{14}N have been limited to biomolecules[66–68] and are thus outside the scope of this article.

Although the theoretical gains in sensitivity for low-γ nuclei are massive, on the order of 10^4, obtaining these enhancements can be very difficult. As mentioned earlier, DNP can be performed using two separate approaches known as direct (i.e., $e^- \rightarrow X$) and indirect DNP (i.e., $e^- \rightarrow {}^1H \rightarrow X$). Direct DNP is clearly the more general approach, as it does not require the presence of an intermediate ^{1}H spin, but can be challenging for low-γ nuclei as much of the enhancement can be lost due to the overlap of the positive and negative enhancement maxima that are separated by only ν_0 for cross-effect DNP and $2\nu_0$ for solid-effect DNP.[69] The long T_1 relaxation times that are commonly observed for these nuclei can help improve the DNP enhancements, but at the cost of an increased recycle delay between scans. Despite this difficulty, direct DNP of ^{25}Mg via the solid effect has been performed at 4.2 K and 1.127 T on a Cr^{3+}-doped Mg_2SiO_4 crystal.[70] More recently, an 835-fold enhancement of an ^{89}Y signal was achieved by direct DNP in a nonspinning YDOTA sample at 1.4 K and 3.35 T.[71] All applications of MAS DNP to low-γ nuclei in materials, however, have opted instead for the use of the indirect DNP approach and have thus focused on the study of hydrogen-containing materials.

The first modern application of DNP for the characterization of materials via low-γ nuclei was performed by Blanc *et al.*,[72] who showed that the ^{89}Y CPMAS spectra of Y^{3+}-containing frozen solutions could be acquired in mere minutes; importantly noting that an added benefit of the cryogenic cooling used in DNP is the efficient heat dissipation during the long high-power spin locking pulses required to achieve the ^{1}H-^{89}Y CP transfer. They also studied ceramics made of hydrated Y-doped zirconate ($BaZrO_3$), a promising proton conductor with potential uses in solid oxide fuel cells. Only low enhancements of ~2–3 could be achieved in this case due to the low ^{1}H density of the material that impedes the ^{1}H–^{1}H spin diffusion. The improved sensitivity nevertheless enabled a ^{89}Y{^{1}H} HETCOR spectrum to be acquired in a reasonable amount of time (15 h), enabling the detection of two different proton-trapping defect sites, which are important in mediating proton conduction.

Recently, ^{89}Y DNP SENS has also been applied to the characterization of silica-supported single-site Y catalysts. First, Eedugurala *et al.*[73] attempted to apply ^{89}Y DNP SENS to directly determine the podality of $Y\{N(SiHMe_2)tBu\}_3$ catalysts grafted onto MSNs that were thermally treated at 550 and 700 °C. Although the slight differences observed between the two catalysts were in agreement with the expected changes in podality, it was later discovered, using ^{15}N DNP SENS, that this catalyst had decomposed under the DNP conditions. More recently, Delley *et al.*[74] applied ^{89}Y DNP SENS on similar single-site catalysts ($Y\{N(SiMe_3)_2\}_3$ and $Y\{OSi(OtBu)_3\}_3\{OHSi(OtBu)_3\}$), again with the goal of elucidating the coordination geometry of the surface-supported Y complexes. With the help of DFT calculations on model compounds, they were able to assign the ^{89}Y chemical shifts and show that tri-, tetra-, and pentacoordinated Y sites could all be found on the silica surface (Figure 5). The addition of nitrogen ligands was shown to slightly increase the ^{89}Y chemical shifts.

One of the most desirable NMR-active isotopes is ^{43}Ca, owing to the importance of Ca in both materials science and biology. Similar to ^{17}O, however, ^{43}Ca NMR is plagued by a combination of very low natural abundance (0.135%) and a low γ value (~15 times smaller than ^{1}H), which has limited the development of ^{43}Ca SSNMR.[76] Nevertheless, due to its small quadrupole moment and high spin quantum number ($I = 7/2$), ^{43}Ca often yields relatively narrow resonances, making it an ideal candidate for study by DNP-enhanced SSNMR.

The earliest ^{43}Ca DNP experiment was performed in 1974 by Abragam *et al.*, who used an indirect ^{19}F–^{43}Ca DNP approach

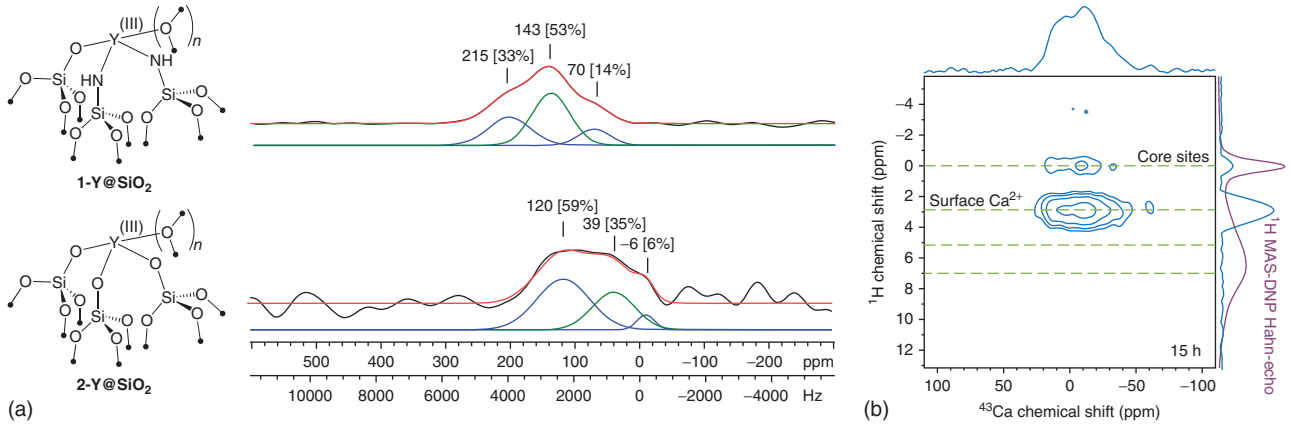

Figure 5. DNP-enhanced NMR data acquired for low-γ nuclei in materials. (a) DNP-enhanced ^{89}Y CP-CPMG MAS NMR spectra of the surface complexes depicted on the left. The spectra are deconvoluted to Y sites with varying coordination numbers. (b) ^{43}Ca{^{1}H} HETCOR spectrum acquired on a carbonated hydroxyapatite sample, with well-resolved resonances from surface and core ^{43}Ca sites. ((a) Reprinted with permission from M. F. Delley, G. Lapadula, F. Núñez-Zarur, A. Comas-Vives, V. Kalendra, G. Jeschke, D. Baabe, M. D. Walter, A. J. Rossini, A. Lesage, L. Emsley, O. Maury and C. Copéret, J. Am. Chem. Soc., 2017, 139, 8855. Copyright 2017 American Chemical Society. (b) Source: Lee *et al.*,[75] https://www.nature.com/articles/ncomms14104. Licensed under CC BY 4.0)

to hyperpolarize and detect the ^{43}Ca NMR signal from a CaF_2 crystal.[77] They first hyperpolarized the ^{19}F nuclei directly by DNP, using a Tm^{2+} dopant as a polarization source, and transferred this hyperpolarization to the ^{43}Ca spins by adiabatic demagnetization in the rotating frame. According to their estimations, they achieved a ^{43}Ca nuclear polarization of $80 \pm 15\%$ using this approach. Surprisingly, only one study has been published using ^{43}Ca DNP-enhanced SSNMR since the technique's recent renaissance.[75] In this study, Lee *et al*. applied indirect ^{1}H–^{43}Ca MAS DNP for the study of hydroxyapatite nanoparticles, an important mineral found in bones. They were able to improve the sensitivity of ^{43}Ca SSNMR by a factor of 35 compared to conventional SSNMR and used a ^{43}Ca{^{1}H} HETCOR experiment to distinguish surface and core ^{43}Ca sites in carbonated hydroxyapatite. Unfortunately, the spectrum was found to be dominated by a surface species that was difficult to identify, perhaps due to poor spin diffusion of hyperpolarization into the bulk. As many important calcium-containing materials, such as ceramics and cements, have either a poor or nonexistent ^{1}H content, further expansion of the capabilities of direct DNP is needed to enable spectroscopic elucidation of bulk sites.

Ultrawideline NMR

Many compounds of interest in materials science contain heavy spin-1/2 nuclei (e.g., ^{195}Pt and ^{207}Pb) or quadrupolar nuclei (e.g., ^{14}N, $^{35/37}$Cl, and $^{79/81}$Br), which yield very broad SSNMR spectra, ranging from several hundred kilohertz to several megahertz, owing to their large CSA or quadrupolar interactions. The resulting spectral dispersion has a detrimental effect on sensitivity, which is often exacerbated by the low γ values and/or low natural abundances of many such nuclei. To date, the vast majority of the applications of DNP to materials have used MAS to average the CSA and the first-order quadrupolar broadening, as well as reduce the second-order quadrupolar broadening of the central transition of half-integer quadrupolar nuclei by a factor of ~3. In studies involving highly disordered materials with inhomogeneously broadened spectra, or in cases where the second-order quadrupolar interaction is simply too large, however, MAS can easily become ineffective, only yielding large manifolds of unresolved spinning sidebands. In such cases, it is often advantageous to acquire the spectra on static samples with the use of modern ultrawideline SSNMR methods. These methods include those making use of frequency-swept wideband, uniform-rate, and smooth-truncation (WURST) pulses to overcome limited excitation bandwidths of square RF pulses.[78] Along these lines, an important development that enables indirect ultrawideline DNP experiments is the broadband adiabatic inversion cross-polarization (BRAIN-CP) experiment. This experiment incorporates a WURST adiabatic inversion pulse in lieu of the spin locking pulse seen in conventional CP to cross-polarize broad lines in static samples.[79] Even with the use of these techniques, however, uniform excitation of broad spectra can rarely be achieved at any single transmitter offset, and thus a piecewise acquisition of ultrawideline spectra using the variable offset cumulative spectrum (VOCS) acquisition method is often required.[80] The sensitivity of these approaches can be further enhanced by detecting the signal with a WURST-based CPMG train of echoes (BRAIN-CP-WCPMG, or BCP).[81]

Recently, DNP has been coupled with the aforementioned BCP technique to further increase the sensitivity of ultrawideline SSNMR.[82–84] For example, Kobayashi *et al.*[82] acquired ultrawideline ^{195}Pt SSNMR spectra of Pt^{2+}-loaded UiO-66-NH_2 MOFs by combining DNP with ^{195}Pt{^{1}H} BCP (Figure 6a). Although the measurement of ^{195}Pt{^{1}H} BCP spectra, spanning over 10 000 ppm, required piecing together 14 subspectra, the final coadded spectrum was obtained in a practicable experimental time of ~7.5 h. The spectral lineshapes, in conjunction with theoretical calculations, revealed the formation of both *cis*- and *trans*-coordinated Pt complexes

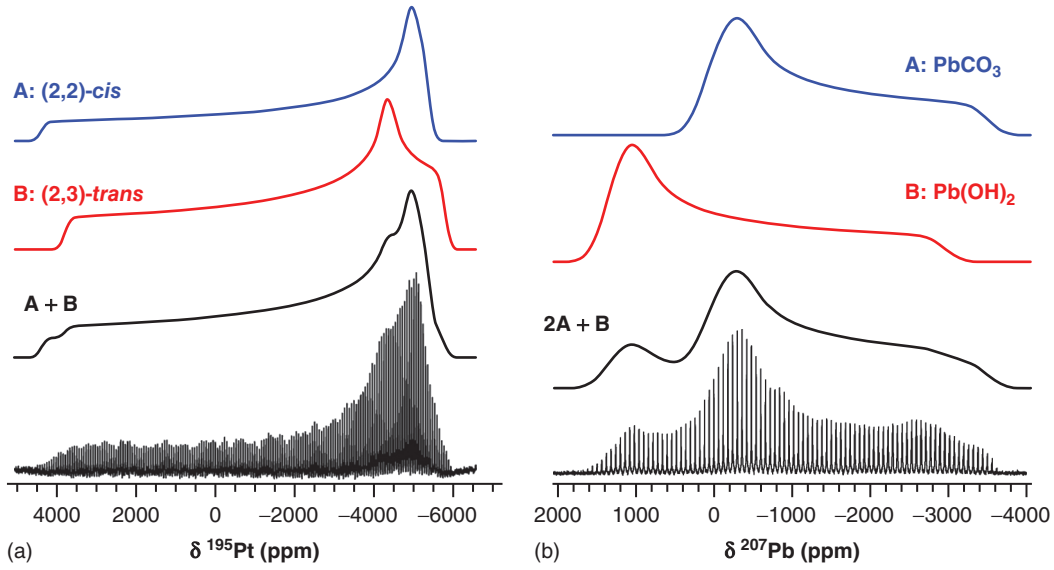

Figure 6. (a) DNP-enhanced ultrawideline ^{195}Pt{^{1}H} BCP spectrum of Pt^{2+}/UiO-66-NH_2 and the simulated powder patterns for the Pt^{2+} cations bound to $-NH_2$ in trans and cis configurations. (b) DNP-enhanced ultrawideline ^{207}Pb{^{1}H} BCP spectrum of basic lead white and its deconvolution into sites A and B in lead carbonate and lead hydroxide layers, respectively. ((a) Reprinted with permission from T. Kobayashi, F. A. Perras, T. W. Goh, T. L. Metz, W. Huang and M. Pruski, J. Phys. Chem. Lett., 2016, 7, 2322. Copyright 2016 American Chemical Society. (b) Reproduced from T. Kobayashi, F. A. Perras, A. Murphy, Y. Yao, J. Catalano, S. A. Centeno, C. Dybowski, N. Zumbulyadis and M. Pruski, Dalton Trans., 2017, 46, 3535 with permission from The Royal Society of Chemistry)

in the UiO-66-NH_2. Notably, this conformational information can only be extracted via the CSA and is unobtainable by MAS-based ^{195}Pt SSNMR spectroscopy, an added value of ultrawideline SSNMR. The $\varepsilon_{on/off}$ factors achieved in this study were on the order of 5, which is considerably less than the values commonly reported for MAS DNP. This is due to the difficulty to satisfy the cross-effect condition in static samples,[85] as well as the fact that UiO-66-NH_2 MOF poses diffusional constraints for the radicals. Interestingly, Kubicki *et al.*[86] observed that the DNP enhancement can be increased by the addition of dielectric particles to the samples. Indeed, mixing the abovementioned Pt^{2+}/UiO-66-NH_2 with NaCl particles (75% w/w) increased the DNP enhancement by an additional factor of 5, which resulted in a higher overall sensitivity than a rotor containing pure Pt^{2+}/UiO-66-NH_2, despite the decreased sample amount.[82]

DNP-enhanced ultrawideline ^{207}Pb SSNMR spectroscopy has also been applied to characterize lead compounds relevant to cultural heritage science.[83] Specifically, DNP-enhanced ^{207}Pb SSNMR measurements enabled, for the first time, the observation of the basic lead carbonate phase in the lead white pigment (Figure 6b). The measurements also detected the formation of a lead soap in an aged paint film, thus demonstrating that this new methodology holds promise for the application of SSNMR to dilute and severely mass-limited archeomaterials and other objects of cultural significance.

Hirsh *et al.* have published the only current example of a DNP-enhanced BCP experiment on a quadrupolar nucleus. Notably, they demonstrated that the low signal enhancement in static samples can, at least in part, be alleviated using a technique dubbed 'spinning-on spinning-off' (SOSO), where the sample is spun to enhance the cross-effect condition during the recycle delay and is stopped for the data acquisition.[84] In favorable cases, using histidine HCl and ambroxol HCl, with sufficiently long ^{1}H T_1 relaxation times to allow for the spinning-down operation, the SOSO approach improved the DNP enhancement by a factor of 2 (Figure 7), but still fell short of the values expected under MAS.

Unlike the case for $I = 1/2$ nuclei, however, an improved sensitivity is not a guarantee for DNP-enhanced BCP spectra of quadrupolar nuclei. The rapid relaxation of quadrupolar nuclei may lead to an improved time performance for direct, non-DNP-enhanced, excitation. For example, Figure 7(a) and (b) show the ultrawideline ^{79}Br SSNMR spectra of 4-bromopyridine hydrobromide acquired using DNP-enhanced ^{79}Br{^{1}H} BCP and conventional ^{79}Br WCPMG, respectively. While the DNP experiment (Figure 7a, $\varepsilon_{on/off} \sim 4$) offered a higher signal intensity per scan than the ^{79}Br WCPMG experiment acquired without DNP (Figure 7b), by a factor of ~5, the time sensitivity of the conventional ^{79}Br WCPMG experiment was double that of the DNP experiment. This result was due to the long recycle delay required for DNP buildup (40 s, vs 0.5 s for WCPMG). Note that a significantly greater sensitivity could have been obtained at an ultrahigh magnetic field (~7.5 at 21.1 T) due to the $B_0^{5/2}$ dependence. Further advances in instrumentation, pulse sequences, and sensitizers that exploit DNP mechanisms other than the cross-effect are expected to expand the applications of ultrawideline DNP-enhanced SSNMR, as seen, for instance, with the improved performance of trityl in static direct ^{17}O DNP experiments.[31]

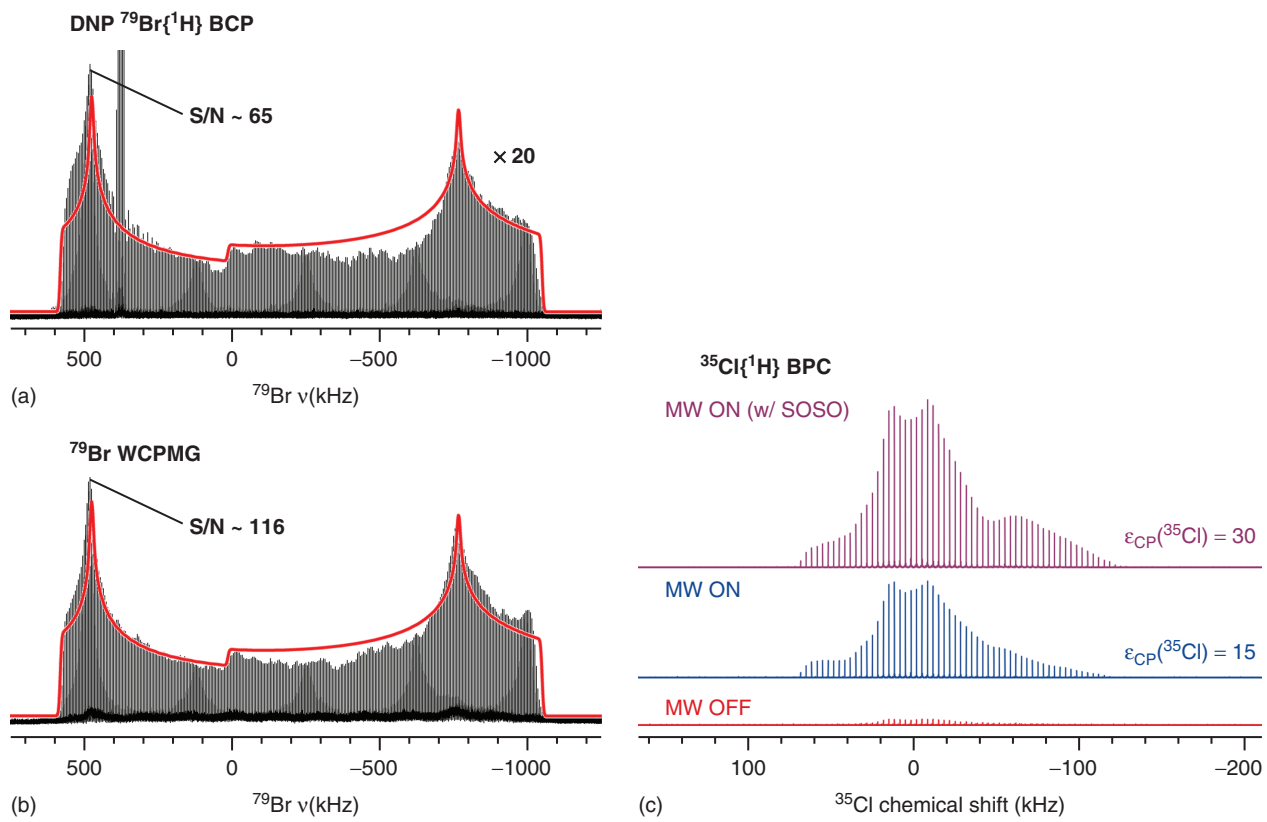

Figure 7. (a,b) ^{79}Br NMR spectra of 4-bromopyridine hydrobromide, obtained using ^{79}Br{^{1}H} DNP-enhanced BCP (a) and ^{79}Br WCPMG without microwave irradiation (b). The two spectra were acquired using equal experiment times and were both normalized to the number of scans. The spectra are fit to $\delta_{iso} = 150 \pm 100$ ppm, $C_Q = 33.2 \pm 0.2$ MHz, and $\eta = 0.15 \pm 0.01$. (c) ^{35}Cl{^{1}H} BPC spectra of ambroxol HCl showing the effect of the SOSO procedure

Correlation Spectroscopy Involving Unreceptive and/or Rare Nuclei

Acquisition of Challenging Homonuclear Correlation Experiments

Perhaps no experiment type better exemplifies DNP's capacity to 'grow signals from the noise' than the acquisition of 2D correlation spectra between rare nuclei, such as ^{13}C or ^{29}Si. Homonuclear and heteronuclear correlation experiments have unrivaled capacity for providing atomic-scale structural insight by determining intra- and intermolecular spin topology. Typically, such experiments involve highly sensitive ^{1}H nuclei, at least in one spectral dimension. Two-dimensional ^{1}H–^{1}H homonuclear correlation experiments have a particular advantage of high sensitivity;[87] however, their applications are often limited by low resolution, arising from the narrow chemical shift range and significant homonuclear dipolar broadening, present even under fast MAS and/or ^{1}H–^{1}H homonuclear decoupling. Heteronuclear ^{1}H–X spectroscopy takes advantage of higher resolution due to the wider chemical shift range of heteronuclei (X) at the expense of reduced sensitivity due to their lower γ and low natural abundance. In addition, the inefficiency of long-range polarization transfers and dipolar truncation effects strongly favor short-range intramolecular ^{1}H–X correlations. Homonuclear X–X spectroscopy, on the other hand, offers the highest resolution but has, until recently, been prohibitively insensitive under natural abundance. Note that the probability of finding an interacting pair of nuclei depends on the product of their natural abundances. The natural abundance ^{29}Si–^{29}Si double-quantum/single-quantum (DQ/SQ) correlation spectra obtained on 'NMR-friendly' crystalline zeolites are among the few examples of such studies reported by conventional NMR.[88–90]

Unprecedented signal enhancements offered by DNP have created new opportunities for the measurement of through-space and through-bond 2D homonuclear correlation spectra between unreceptive and low natural abundance nuclei within a practical experimental time.[49,91–101] In fact, some of these studies raised the sensitivity bar even higher by measuring correlation spectra of species that constituted only a fraction of the surface.[49,95,97,99,101] For example, both through-space and through-bond 2D DQ/SQ ^{29}Si–^{29}Si correlation spectra of a self-condensed organosiloxane layer formed on silica nanoparticles could be observed within a reasonable experimental time (Figure 8b).[95] The correlation spectra provided structural insights into the polymerization of organosiloxanes grafted onto silica nanoparticles; the modifier produced laterally self-condensed functionalizing groups without yielding significant core–shell oligomers above the surface.

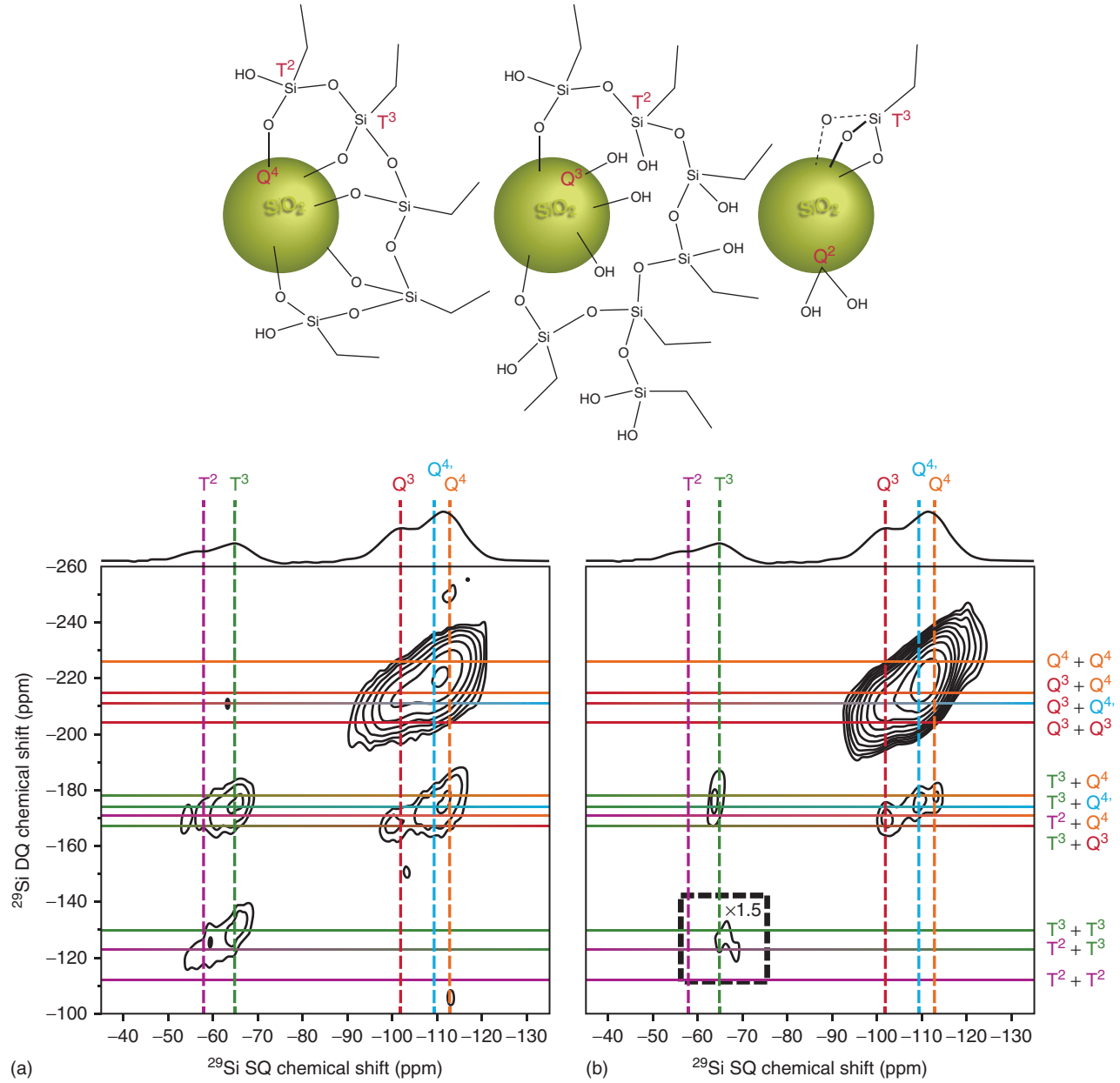

Figure 8. DNP-enhanced ^{29}Si–^{29}Si DQ/SQ correlation spectra of the polyethylsiloxane-functionalized silica nanoparticles via through-space dipolar coupling with the POST-C7 sequence (a), and through-bond scalar coupling with the INADEQUATE sequence (b). Each 2D experiment was recorded in ~5.5 h. (Reprinted with permission from D. Lee, G. Monin, N. T. Duong, I. Z. Lopez, M. Bardet, V. Mareau, L. Gonon and G. De Paëpe, J. Am. Chem. Soc., 2014, 136, 13781. Copyright 2014 American Chemical Society, https://pubs.acs.org/doi/abs/10.1021/ja506688m)

We recently applied similar DNP-enhanced ^{29}Si–^{29}Si homonuclear correlation experiments to shed light on the long-standing conundrum regarding the spatial distribution of organic functional groups attached to the surface of MSNs via cocondensation and postsynthesis grafting of organosilane precursors.[97] The study established that T^3–T^3 site correlations could be observed in the DQ/SQ spectrum of cocondensed samples (Figure 9a), but not in the spectra of grafted samples (Figure 9b), unambiguously demonstrating that, contrary to some earlier reports, the latter synthetic method leads to a more homogeneous distribution of surface groups. Evidently, the organosilane precursors do not self-condense during the anhydrous grafting process, and are unlikely to bond to the silica surface in close proximity (<4 Å) due to the scarcity of suitably arranged hydroxyl groups.

We subsequently applied DNP-enhanced ^{13}C–^{13}C homonuclear correlation spectroscopy to detect intermolecular interactions between two types of MSN-bound organic functional groups: phenyl (Ph) and mercaptopropyl (MP).[100] Note that with the natural ^{13}C abundance of 1.1%, only 1 out of 8300 C–C pairs can produce correlation signals. The detection of ^{13}C–^{13}C correlations between species dispersed

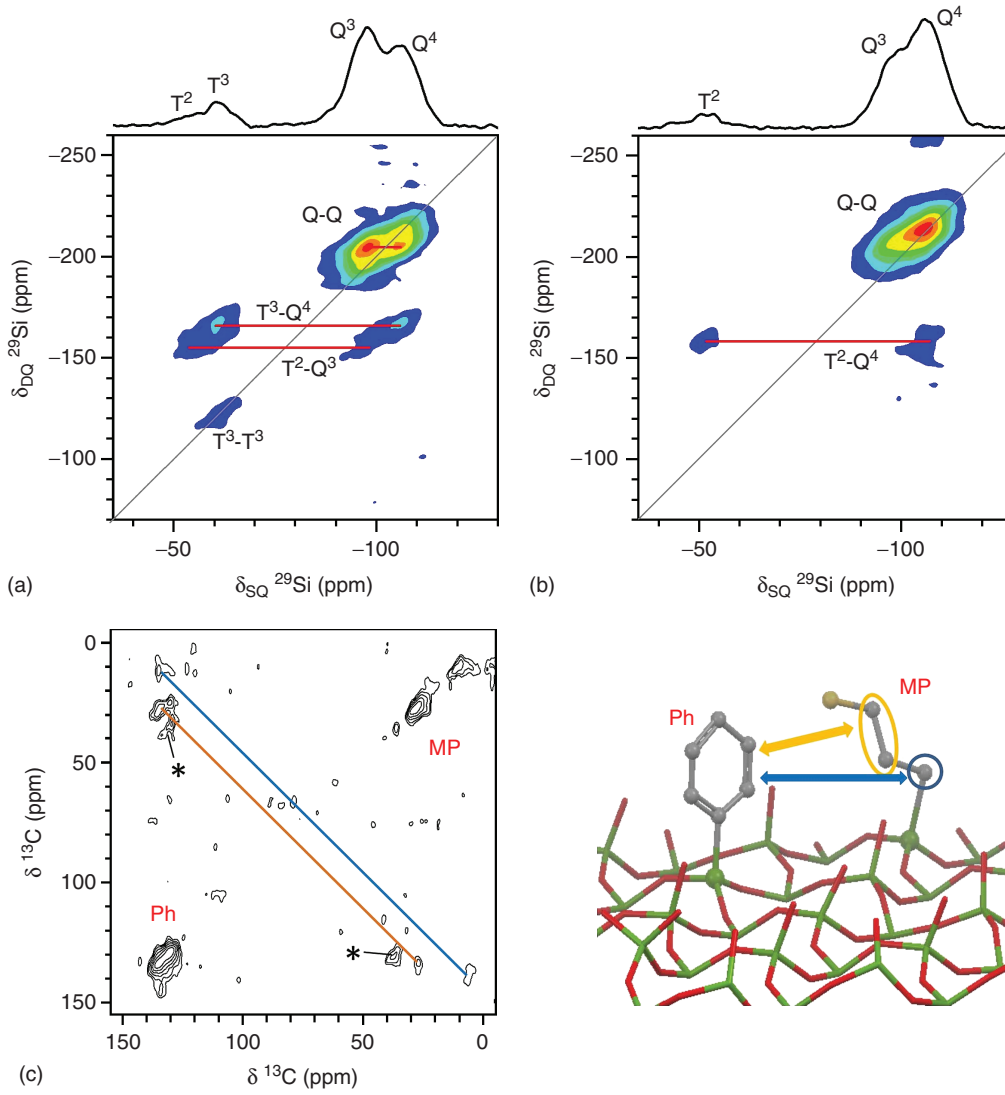

Figure 9. DNP-enhanced 2D ^{29}Si–^{29}Si DQ/SQ correlation spectra of mercaptopropyl-functionalized MSNs synthesized via cocondensation (a) and grafting (b), obtained using 5.3 ms of SPC-5 recoupling. (c) DNP-enhanced 2D ^{13}C–^{13}C SQ/SQ correlation spectrum of MP/Ph-bifunctionalized MSNs obtained using 200 μs of mixing time in the CHHC scheme. ((a,b) Reproduced from T. Kobayashi, D. Singappuli-Arachchige, Z. Wang, I. I. Slowing and M. Pruski, Phys. Chem. Chem. Phys., 2017, 19, 1781 with permission from The Royal Society of Chemistry. (c) Reprinted with permission from T. Kobayashi, I.I. Slowing, and M. Pruski, J. Phys. Chem. C, 2017, 121, 24687. Copyright 2017 American Chemical Society)

on the surface further exacerbates the sensitivity challenge. Nevertheless, the SQ/SQ ^{13}C–^{13}C homonuclear correlation experiment known as CP3 or CHHC, which relies on X-edited ^{1}H spin diffusion,[102,103] successfully detected the intermolecular Ph–MP correlations (Figure 9c) on MSN surfaces. This approach can also be applied for other combinations of nuclei, such as CHHN.

The ability to measure homonuclear correlation spectra under natural abundance adds the benefit of circumventing dipolar truncation effects, thereby allowing the measurement of long-range interactions and distances. For example, ^{13}C–^{13}C distances of up to 0.7 nm were measured in a self-assembled cyclic diphenylaniline peptide using DNP-enhanced ^{13}C–^{13}C DQ buildup curves.[13] In addition, such long-range correlations do not suffer from the broadening caused by one-bond scalar couplings, which improves the spectral resolution. Indeed, the DNP-enhanced ^{13}C–^{13}C correlation techniques can be used to access structural constraints, which are unavailable in isotopically-labeled systems owing to dipolar truncation effects. These structural parameters can in turn be used to elucidate the intermolecular order in organic compounds that cannot be prepared in a crystalline form suitable for X-ray diffraction, opening the door to *de novo* NMR crystallography.[49,95,101]

Acquisition of Challenging Heteronuclear Correlation Experiments

DNP has also been applied in a number of cases for the acquisition of very challenging heteronuclear correlation experiments involving rare nuclear isotopes in materials. As in the homonuclear case, the sensitivity of many of these

experiments can be remarkably low given that the intensity depends on the multiplication of the natural abundances of the two isotopes and is further reduced by a factor of $(2I)^{-1}$ for half-integer quadrupolar nuclei. The first such DNP-facilitated heteronuclear correlation experiment in materials, excluding ^{1}H-correlated experiments, was the ^{13}C{^{27}Al} dipolar–heteronuclear multiple-quantum correlation (D-HMQC)[104] spectrum acquired for MIL-100(Al) MOF.[105] In this case, >90% of the polarization was lost due to recoupling inefficiencies and satellite transition magnetization.

Piveteau *et al.*[106] have used DNP to enhance the ^{125}Te, $^{111/113}$Cd, ^{77}Se, and ^{31}P SSNMR signals from InP, CdSe, PbSe, CdTe, and PbTe quantum dots. In the case of InP quantum dots, they were able to observe the signals from an oxidized surface, whereas separate core and shell ^{113}Cd resonances were observed for the CdSe sample. In order to assign these resonances, they performed a ^{13}C{^{111}Cd} D-HMQC experiment, showing that the carboxylate carbon of the oleate capping surfactant was in close proximity to one of the Cd sites, which also featured a far greater CSA. They thus concluded that this quantum dot had a core–shell structure with crystalline CdSe in the core and a surface that is capped by oleate ligands. The key to the success of this study was the dispersion of the quantum dots into mesoporous silica, which prevented their agglomeration and facilitated close contact between the polarizing agent and the quantum dot surface.

Silica-aluminas are important solid Brønsted acid catalysts of use in industry; however, the lack of crystallinity of these materials has prevented their characterization by crystallographic methods. As a result, much of their structure is unknown, and the nature of their Brønsted acidic sites has been hotly debated.[107] Using DNP, Valla *et al.*,[108] as well as Rankin *et al.*[109] in a later publication, were able to acquire challenging through-bond (refocused-INEPT) as well as through-space (D-INEPT) ^{27}Al{^{29}Si} correlation spectra on silicated alumina (Si/Al_2O_3) and aluminated silica (Al/SiO_2) (Figure 10). They found that, in general, the through-bond Si–O–Al linkages were predominantly to tetrahedral aluminum sites, while correlations to higher coordination numbers were observed in the through-space correlation spectra, particularly as the aluminum content increased. This led to the conclusion that the Brønsted acidic sites are associated with four-coordinate aluminum.

Aside from chemical shift correlation experiments, DNP has also enabled difficult heteronuclear dipolar recoupling experiments that have yielded unprecedented insights into the three-dimensional arrangements of atoms on surfaces. The potential of DNP to enable such difficult experiments was demonstrated by Pourpoint *et al.*, who used it to considerably accelerate, and improve the quality of, ^{13}C{^{27}Al} rotational-echo saturation pulse double-resonance (RESPDOR)[110] experiments performed on MIL-100(Al) MOF.[105] Perras *et al.*[111] later built on this work and managed to obtain high-quality ^{13}C{^{27}Al} RESPDOR curves for the organic species situated at the surfaces of alumina and alumina-supported Pd catalysts. A novel simulation strategy was developed to accurately calculate the RESPDOR dephasing curves as a function of the distance between individual carbon atoms

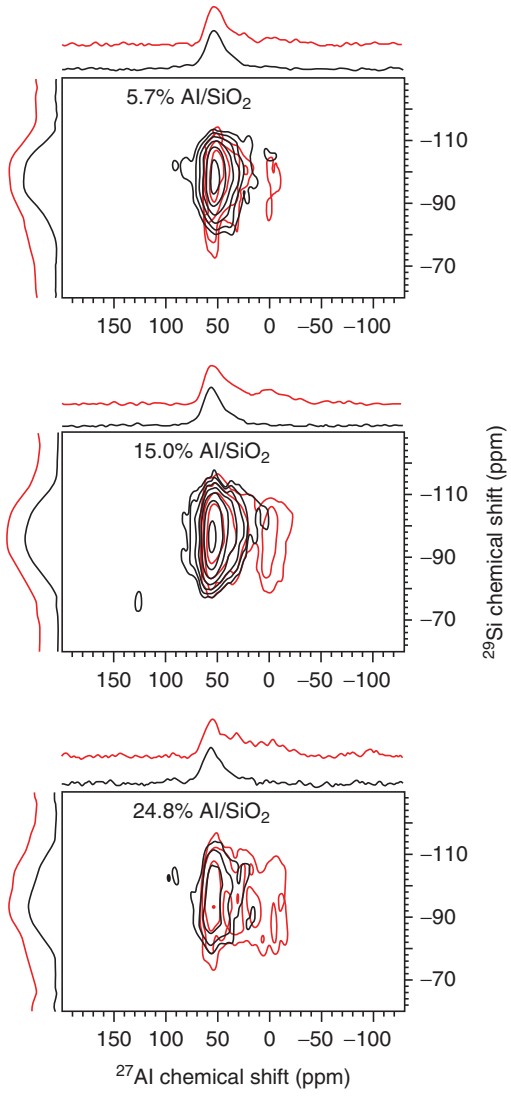

Figure 10. ^{27}Al{^{29}Si} refocused-INEPT (black) and D-INEPT (red) HETCOR spectra of aluminated silicas, with the aluminum content indicated on the spectra. The four-coordinate Al sites bind to the silica, while larger quantities of six-coordinate Al are situated near the silica as the aluminum concentration is increased. (Reprinted with permission from M. Valla, A. J. Rossini, M. Caillot, C. Chizallet, P. Raybaud, M. Digne, A. Chaumonnot, A. Lesage, L. Emsley, J. A. van Bokhoven and C. Copéret, J. Am. Chem. Soc., 2015, 137, 10710. Copyright 2014 American Chemical Society, https://pubs.acs.org/doi/abs/10.1021%2Fjacs.5b06134)

and the γ-Al_2O_3 surface. As a result, they were able to measure the distances between individual sites in methionine and a polyvinyl alcohol (PVA) coating to the catalyst support surface and determine their 3D conformations. This study showed that methionine, which is a catalyst poison, coordinates to an aluminum site at the surface and lays prone on the surface. Most notably, in the presence of Pd, methionine coordinates with the support, whereas the sulfur group bonds to the nanoparticle; this bimodal coordination to the catalyst likely exacerbates the poisoning effect of the compound (Figure 11). By contrast, the PVA chains were

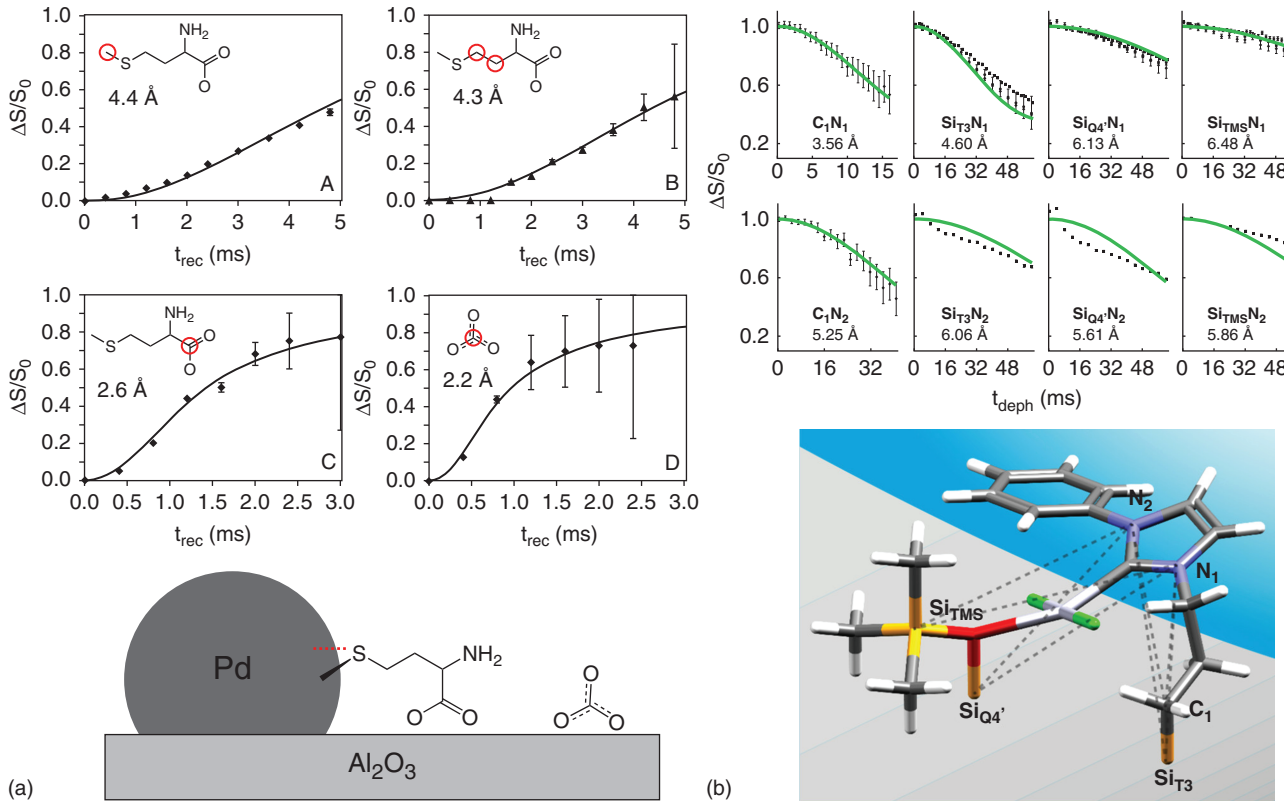

Figure 11. Dipolar recoupling measurements performed to determine the conformations of surface species. In (a) $^{13}C\{^{27}Al\}$ RESPDOR measurements were performed to extract the distance of individual carbon sites from the surface of the alumina support. Methionine was found to coordinate to both the alumina support and the Pd nanoparticle surface and to lay prone on the surface. In (b) $^{13}C\{^{15}N\}$ and $^{29}Si\{^{15}N\}$ REDOR measurements were performed to determine the 3D structure of a Pt complex; the best-fit structure is depicted on the bottom. ((a) Reprinted with permission from F. A. Perras, J. D. Padmos, R. L. Johnson, L.-L. Wang, T. J. Schwartz, T. Kobayashi, J. H. Horton, J. A. Dumesic, B. H. Shanks, D. D. Johnson and M. Pruski, J. Am. Chem. Soc., 2017, 139, 2702. Copyright 2017 American Chemical Society. (b) Reprinted with permission from P. Berruyer, M. Lelli, M. P. Conley, D. L. Silverio, C. M. Widdifield, G. Siddiqi, D. Gajan, A. Lesage, C. Copéret and L. Emsley, J. Am. Chem. Soc., 2017, 139, 849. Copyright 2017 American Chemical Society)

shown to interact with the surface through hydrogen-bonding interactions.

Sangodkar *et al.*[112] have used a similar strategy to establish the interactions between sucrose and tricalcium silicate, which is the primary constituent of Portland cement. Using $^{29}Si\{^{13}C\}$ rotational echo double-resonance (REDOR) experiments,[113] they were able to show that sucrose preferentially adsorbs onto Q^1 and Q^2 sites and slows the growth of calcium silicate hydrate chains that are responsible for the strength of concrete.

Finally, REDOR experiments were applied to determine the high-resolution 3D structures of single-site catalysts on silica surfaces. For example, DNP-enhanced $^{13}C\{^{119}Sn\}$ REDOR measurements were carried out on butyltin organometallic complexes grafted onto a silica support to confirm that the butyl ligands were indeed bound to the Sn site.[63] Impressively, these experiments were performed at natural isotopic abundance and correspond to the detection of only 0.09% of all carbon-tin pairs in a surface-supported complex. More recently, Berruyer *et al.*[55] have used extensive $^{13}C\{^{15}N\}$ and $^{29}Si\{^{15}N\}$ REDOR measurements, in conjunction with extended X-ray absorption fine structure (EXAFS), to extract a large number of nontrivial structural constraints on a silica-supported organometallic Pt complex. The three-dimensional structure of this complex was then fit directly to the REDOR data (Figure 11). It was then discovered that all the conformations that were in good agreement with experiment were very similar, which led to the conclusion that this complex may feature a well-defined three-dimensional structure on the surface.

Concluding Remarks

DNP has revolutionized the SSNMR spectroscopy of materials and is pushing back the limits of what was once thought to be impossible. In just a few years, we have seen a number of previously unthinkable SSNMR experiments performed with great success, such as the acquisition of natural abundance ^{15}N, ^{17}O, and ^{43}Ca spectra from surfaces. Similarly, ^{29}Si–^{29}Si and even ^{13}C–^{13}C correlations have been observed from the surfaces of mesoporous materials. Such experiments open the door to far greater insights into material structures and functions than was possible only a decade ago. Undoubtedly, the list of experiments and nuclides that still remain beyond our grasp will continue to shrink in the coming decade with the continued development of ultralow-temperature and pulsed DNP, which promise to further 'grow SSNMR signals from the noise'.

Acknowledgments

This research is supported by the U.S. Department of Energy, Office of Basic Energy Sciences, Division of Chemical Sciences, Geosciences, and Biosciences through the Ames Laboratory. The Ames Laboratory is operated for the U.S. Department of Energy by Iowa State University under Contract No. DE-AC02-07CH11358. F.P. thanks the Natural Sciences and Engineering Research Council of Canada and the Government of Canada for a Banting Fellowship.

Biographical Sketches

Frédéric A. Perras. b. 1988. BSc (Hons), 2010, University of Ottawa; PhD, 2014, University of Ottawa (with D. L. Bryce). Spedding (2015–2017) and Banting (2016–2018) postdoctoral fellow, Ames Laboratory (with M. Pruski). Associate scientist at the Ames Laboratory, 2018–present. Approx. 50 publications. Research interests include solid-state NMR of quadrupolar nuclei, NMR studies of materials, heterogeneous catalysis, spin dynamics and spectral simulation, and magic-angle-spinning dynamic nuclear polarization.

Takeshi Kobayashi. b. 1968. BSc 1992, Tokyo University of Science; PhD 2001, Nagasaki University (with Y. Teraoka). Assistant Professor, the University of Tokyo (2002–2004). Postdoctoral fellow at the University of Illinois at Urbana-Champaign (with A. Wieckowski and E. Oldfield, 2004–2005), Colorado State University (with G. E. Maciel, 2006–2009), and Ames Laboratory (with M. Pruski, 2010–2011). Associate Scientist, Ames Laboratory, 2011–present. Approx. 80 publications. Current research interests: solid-state NMR, including dynamic nuclear polarization studies of materials, especially molecular interactions on surfaces, and quantum chemical interpretation of NMR parameters.

Marek Pruski. b. 1954. MS, 1977; PhD, 1981, N. Copernicus University, Torun, Poland. Introduced to NMR in 1982 at the N. Copernicus University and Universität Leipzig. Postdoctoral fellow at the Iowa State University (with B.C. Gerstein), 1985–1988. Currently senior scientist and adjunct professor of chemistry, Ames Laboratory, Iowa State University. Approx. 210 publications. Research interests: solid-state NMR and its applications to surface and material sciences, high-resolution correlation methods for half-integer quadrupolar and spin-1/2 nuclei, fast magic angle spinning, and dynamic nuclear polarization.

Related Articles

Dynamic Nuclear Polarization and High-Resolution NMR of Solids

References

1. A. B. Barnes, M. L. Mak-Jurkauskas, Y. Matsuki, V. S. Bajaj, P. C. A. van der Wel, R. DeRocher, J. Bryant, J. R. Sirigiri, R. J. Temkin, J. Lugtenburg, J. Herzfeld, and R. G. Griffin, *J. Magn. Reson.*, 2009, **198**, 261.
2. L. R. Becerra, G. J. Gerfen, B. F. Bellew, J. A. Bryant, D. A. Hall, S. J. Inati, R. T. Weber, S. Un, T. F. Prisner, A. E. McDermott, K. W. Fishbein, K. E. Kreischer, R. J. Temkin, D. J. Singel, and R. G. Griffin, *J. Magn. Reson. Ser. A*, 1995, **117**, 28.
3. K. N. Hu, H.-h. Yu, T. M. Swager, and R. G. Griffin, *J. Am. Chem. Soc.*, 2004, **126**, 10844.
4. Y. Matsuki, T. Maly, O. Ouari, H. Karoui, F. Le Moigne, E. Rizzato, S. Lyubenova, J. Herzfeld, T. Prisner, P. Tordo, and R. G. Griffin, *Angew. Chem. Int. Ed.*, 2009, **48**, 4996.
5. C. Sauvée, M. Rosay, G. Casano, F. Aussenac, R. T. Weber, O. Ouari, and P. Tordo, *Angew. Chem. Int. Ed.*, 2013, **52**, 10858.
6. A. Zagdoun, G. Casano, O. Ouari, M. Schwarzwälder, A. J. Rossini, F. Aussenac, M. Yulikov, G. Jeschke, C. Copéret, A. Lesage, P. Tordo, and L. Emsley, *J. Am. Chem. Soc.*, 2013, **135**, 12790.
7. R. A. Wind, eMagRes, 2007. doi:10.1002/9780470034590.emrstm0140.
8. T. Kobayashi, O. Lafon, A. S. L. Thankamony, I. I. Slowing, K. Kandel, D. Carnevale, V. Vitzthum, H. Vezin, J.-P. Amoureux, G. Bodenhausen, and M. Pruski, *Phys. Chem. Chem. Phys.*, 2013, **15**, 5553.
9. F. Mentink-Vigier, S. Paul, D. Lee, A. Feintuch, S. Hediger, S. Vega, and G. De Paepe, *Phys. Chem. Chem. Phys.*, 2015, **17**, 21824.
10. S. E. Ashbrook and M. E. Smith, eMagres, 2011. doi:10.1002/9780470034590.emrstm1213.
11. G. Wu, *Prog. Nucl. Magn. Reson. Spectrosc.*, 2008, **52**, 118.
12. I. P. Gerothanassis, *Prog. Nucl. Magn. Reson. Spectrosc.*, 2010, **57**, 1.
13. I. P. Gerothanassis, *Prog. Nucl. Magn. Reson. Spectrosc.*, 2010, **56**, 95.
14. I. Hung, G. Wu, and Z. Gan, *Solid State Nucl. Magn. Reson.*, 2017, **84**, 14.
15. F. A. Perras and D. L. Bryce, *J. Phys. Chem. C*, 2012, **116**, 19472.
16. C. P. Romao, F. A. Perras, U. Werner-Zwanziger, J. A. Lussier, K. J. Miller, C. M. Calahoo, J. W. Zwanziger, M. Bieringer, B. A. Marinkovic, D. L. Bryce, and M. A. White, *Chem. Mater.*, 2015, **27**, 2633.
17. S. E. Ashbrook and I. Farnan, *Solid State Nucl. Magn. Reson.*, 2004, **26**, 105.
18. E. Brun, B. Derighetti, E. E. Hundt, and H. H. Niebuhr, *Phys. Lett. A*, 1970, **31**, 416.
19. V. K. Michaelis, E. Markhasin, E. Daviso, J. Herzfeld, and R. G. Griffin, *J. Phys. Chem. Lett.*, 2012, **3**, 2030.
20. C. Song, K.-N. Hu, C.-G. Joo, T. M. Swager, and R. G. Griffin, *J. Am. Chem. Soc.*, 2006, **128**, 11385.
21. F. H. Larsen, H. J. Jakobsen, P. D. Ellis, and N. C. Nielsen, *J. Phys. Chem. A*, 1997, **101**, 8597.
22. F. Blanc, L. Sperrin, D. A. Jefferson, S. Pawsey, M. Rosay, and C. P. Grey, *J. Am. Chem. Soc.*, 2013, **135**, 2975.
23. A. P. M. Kentgens and R. Verhagen, *Chem. Phys. Lett.*, 1999, **300**, 435.
24. F. A. Perras, J. Viger-Gravel, K. M. N. Burgess, and D. L. Bryce, *Solid State Nucl. Magn. Reson.*, 2013, **51–52**, 1.
25. F. A. Perras, T. Kobayashi, and M. Pruski, *J. Am. Chem. Soc.*, 2015, **137**, 8336.
26. X. Zhao, W. Hoffbauer, J. S. auf der Günne, and M. H. Levitt, *Solid State Nucl. Magn. Reson.*, 2004, **26**, 57.
27. F. A. Perras, U. Chaudhary, I. I. Slowing, and M. Pruski, *J. Phys. Chem. C*, 2016, **120**, 11535.
28. A. Gansmüller, J. P. Simorre, and S. Hediger, *J. Magn. Reson.*, 2013, **234**, 154.
29. F. A. Perras, Z. Wang, P. Naik, I. I. Slowing, and M. Pruski, *Angew. Chem. Int. Ed.*, 2017, **56**, 9165.
30. E. P. Parry, *J. Catal.*, 1963, **2**, 371.
31. V. K. Michaelis, B. Corzilius, A. A. Smith, and R. G. Griffin, *J. Phys. Chem. B*, 2013, **117**, 14894.
32. M. A. Hope, D. M. Halat, P. C. M. M. Magusin, S. Paul, L. Peng, and C. P. Grey, *Chem. Commun.*, 2017, **53**, 2142.
33. N. J. Brownbill, D. Gajan, A. Lesage, L. Emsley, and F. Blanc, *Chem. Commun.*, 2017, **53**, 2563.
34. T. V. Can, M. A. Caporini, F. Mentink-Vigier, B. Corzilius, J. J. Walish, M. Rosay, W. E. Maas, M. Baldus, S. Vega, T. M. Swager, and R. G. Griffin, *J. Chem. Phys.*, 2014, **141**, 064202.
35. T. Kobayashi, Y. Nishiyama, and M. Pruski, in Modern Methods in Solid-State NMR, ed. P. Hodgkinson, RSC Publishing: London, 2018.
36. A. Zagdoun, G. Casano, O. Ouari, G. Lapadula, A. J. Rossini, M. Lelli, M. Baffert, D. Gajan, L. Veyre, W. E. Maas, M. Rosay, R. T. Weber, C. Thieuleux, C. Copéret, A. Lesage, P. Tordo, and L. Emsley, *J. Am. Chem. Soc.*, 2012, **134**, 2284.

37. N. Eedugurala, Z. Wang, U. Chaundhary, N. Nelson, K. Kandel, T. Kobayashi, I. I. Slowing, M. Pruski, and A. D. Sadow, *ACS Catal.*, 2015, **5**, 7399.

38. T. Gutmann, J. Liu, N. Rothermel, Y. Xu, E. Jaumann, M. Werner, H. Breitzke, S. T. Sigurdsson, and G. Buntkowsky, *Chem. Eur. J.*, 2015, **21**, 3798.

39. B. Hamzaoui, A. Bendjeriou-Sedjerari, E. Pump, E. Abou-Hamad, R. Sougrat, A. Gurinov, K.-W. Huang, D. Gajan, A. Lesage, L. Emsley, and J.-M. Basset, *Chem. Sci.*, 2016, **7**, 6099.

40. G. S. Foo, J. J. Lee, C.-H. Chen, S. E. Hayes, C. Sievers, and C. W. Jones, *ChemSusChem*, 2017, **10**, 266.

41. J. Liu, P. B. Groszewicz, Q. Wen, A. S. L. Thankamony, B. Zhang, U. Kunz, G. Sauer, Y. Xu, T. Gutmann, and G. Buntkowsky, *J. Phys. Chem. C*, 2017, **121**, 17409.

42. T. Kobayashi, F. A. Perras, U. Chaudhary, I. I. Slowing, W. Huang, A. D. Sadow, and M. Pruski, *Solid State Nucl. Magn. Reson.*, 2017, **87**, 38.

43. A. J. Rossini, A. Zagdoun, M. Lelli, J. Canivet, S. Aguado, O. Ouari, P. Tordo, M. Rosay, W. E. Maas, C. Copéret, D. Farrusseng, L. Emsley, and A. Lesage, *Angew. Chem. Int. Ed.*, 2012, **51**, 123.

44. Z. Guo, T. Kobayashi, L.-L. Wang, T. W. Goh, C. Xiao, M. A. Caporini, M. Rosay, D. D. Johnson, M. Pruski, and W. Huang, *Chem. Eur. J.*, 2014, **20**, 16308.

45. W. R. Grüning, A. J. Rossini, A. Zagdoun, D. Gajan, A. Lesage, L. Emsley, and C. Copéret, *Phys. Chem. Chem. Phys.*, 2013, **15**, 13270.

46. T. K. Todorova, X. Rozanska, C. Gervais, A. Legrand, L. N. Ho, P. Berruyer, A. Lesage, L. Emsley, D. Farrusseng, J. Canivet, and C. Mellot-Draznieks, *Chem. Eur. J.*, 2016, **22**, 16531.

47. F. Blanc, S. Y. Chong, T. O. McDonald, D. J. Adams, S. Pawsey, M. A. Caporini, and A. I. Cooper, *J. Am. Chem. Soc.*, 2013, **135**, 15290.

48. T. Kobayashi, S. Gupta, M. A. Caporini, V. K. Pecharsky, and M. Pruski, *J. Phys. Chem. C*, 2014, **118**, 19548.

49. K. Marker, M. Pingret, J.-M. Mouesca, D. Gasparutto, S. Hediger, and G. De Paëpe, *J. Am. Chem. Soc.*, 2015, **137**, 13796.

50. L. Zhao, I. Smolarkiewicz, H.-H. Limbach, H. Breitzke, K. Pogorzelec-Glaser, R. Pankiewicz, J. Tritt-Goc, T. Gutmann, and G. Buntkowsky, *J. Phys. Chem. C*, 2016, **120**, 19574.

51. J. C. Mohandas, E. Abou-Hamad, E. Callens, M. K. Samantaray, D. Gajan, A. Gurinov, T. Ma, S. Ould-Chikh, A. S. Hoffman, B. C. Gates, and J.-M. Basset, *Chem. Sci.*, 2017, **8**, 5650.

52. M. Werner, A. Heil, N. Rothermel, H. Breitzke, P. B. Groszewicz, A. S. Thankamony, T. Gutmann, and G. Buntkowsky, *Solid State Nucl. Magn. Reson.*, 2015, **72**, 73.

53. A. S. L. Thankamony, C. Lion, F. Pourpoint, B. Singh, A. J. P. Linde, D. Carnevale, G. Bodenhausen, H. Vezin, O. Lafon, and V. Polshettiwar, *Angew. Chem. Int. Ed.*, 2015, **54**, 2190.

54. J. Leclaire, G. Poisson, F. Ziarelli, G. Pepe, F. Fotiadu, F. M. Paruzzo, A. J. Rossini, J.-N. Dumez, B. Elena-Herrmann, and L. Emsley, *Chem. Sci.*, 2016, **7**, 4379.

55. P. Berruyer, M. Lelli, M. P. Conley, D. L. Silverio, C. M. Widdifield, G. Siddiqi, D. Gajan, A. Lesage, C. Copéret, and L. Emsley, *J. Am. Chem. Soc.*, 2017, **139**, 849.

56. L. Protesescu, A. J. Rossini, D. Kriegner, M. Valla, A. de Kergommeaux, M. Walter, K. V. Kravchyk, M. Nachtegaal, J. Stangl, B. Malaman, P. Reiss, A. Lesage, L. Emsley, C. Copéret, and M. V. Kovalenko, *ACS Nano*, 2014, **8**, 2639.

57. W. R. Gunther, V. K. Michaelis, M. A. Caporini, R. G. Griffin, and Y. Roman-Leshkov, *J. Am. Chem. Soc.*, 2014, **136**, 6219.

58. P. Wolf, M. Valla, A. J. Rossini, A. Comas-Vives, F. Núñez-Zarur, B. Malaman, A. Lesage, L. Emsley, C. Copéret, and I. Hermans, *Angew. Chem. Int. Ed.*, 2014, **53**, 10179.

59. P. Wolf, M. Valla, F. Núñez-Zarur, A. Comas-Vives, A. J. Rossini, C. Firth, H. Kallas, A. Lesage, L. Emsley, C. Copéret, and I. Hermans, *ACS Catal.*, 2016, **6**, 4047.

60. J. W. Harris, W.-C. Liao, J. R. Di Iorio, A. M. Henry, T.-C. Ong, A. Comas-Vives, C. Copéret, and R. Gounder, *Chem. Mater.*, 2017, **29**, 8824.

61. Z. Gan, *J. Am. Chem. Soc.*, 1992, **114**, 8307.

62. W.-C. Liao, T.-C. Ong, D. Gajan, F. Bernada, C. Sauvée, M. Yulikov, M. Pucino, R. Schowner, M. Schwarzwälder, M. R. Buchmeiser, G. Jeschke, P. Tordo, O. Ouari, A. Lesage, L. Emsley, and C. Copéret, *Chem. Sci.*, 2017, **8**, 416.

63. M. P. Conley, A. J. Rossini, A. Comas-Vives, M. Valla, G. Casano, O. Ouari, P. Tordo, A. Lesage, L. Emsley, and C. Copéret, *Phys. Chem. Chem. Phys.*, 2014, **16**, 17822.

64. M. E. Smith, *Annu. Rep. NMR Spectrosc.*, 2001, **43**, 121.

65. N. G. Dowell, S. E. Ashbrook, and S. Wimperis, *J. Phys. Chem. B*, 2004, **108**, 13292.

66. V. Vitzthum, M. A. Caporini, and G. Bodenhausen, *J. Magn. Reson.*, 2010, **205**, 177.

67. A. J. Rossini, L. Emsley, and L. A. O'Dell, *Phys. Chem. Chem. Phys.*, 2014, **16**, 12890.

68. J. A. Jarvis, I. Haies, M. Lelli, A. J. Rossini, I. Kuprov, M. Carravetta, and P. T. F. Williamson, *Chem. Commun.*, 2017, **53**, 12116.

69. T. Maly, G. T. Debelouchina, V. S. Bajaj, K.-N. Hu, C.-G. Joo, M. L. Mak-Jurkauskas, J. R. Sirigiri, P. C. A. van der Wel, J. Herzfeld, R. J. Temkin, and R. G. Griffin, *J. Chem. Phys.*, 2008, **128**, 052211.

70. B. Derighetti, S. Hafner, H. Marxer, and H. Rager, *Phys. Lett. A*, 1978, **66**, 150.

71. L. Lumata, A. K. Jindal, M. E. Merritt, C. R. Malloy, A. D. Sherry, and Z. Kovacs, *J. Am. Chem. Soc.*, 2011, **133**, 8673.

72. F. Blanc, L. Sperrin, D. Lee, R. Dervisoğlu, Y. Yamazaki, S. M. Haile, G. De Paëpe, and C. P. Grey, *J. Phys. Chem. Lett.*, 2014, **5**, 2431.

73. N. Eedugurala, Z. Wang, K. Yan, K. C. Boteju, U. Chaudhary, T. Kobayashi, A. Ellern, I. I. Slowing, M. Pruski, and A. D. Sadow, *Organometallics*, 2017, **36**, 1142.

74. M. F. Delley, G. Lapadula, F. Núñez-Zarur, A. Comas-Vives, V. Kalendra, G. Jeschke, D. Baabe, M. D. Walter, A. J. Rossini, A. Lesage, L. Emsley, O. Maury, and C. Copéret, *J. Am. Chem. Soc.*, 2017, **139**, 8855.

75. D. Lee, C. Leroy, C. Crevant, L. Bonhomme-Coury, F. Babonneau, D. Laurencin, C. Bonhomme, and G. De Paëpe, *Nat. Commun.*, 2017, **8**, 14104.

76. D. L. Bryce, *Dalton Trans.*, 2010, **39**, 8593.

77. J. F. Jacquinot, W. T. Wenckebach, M. Goldman, and A. Abragam, *Phys. Rev. Lett.*, 1974, **32**, 1096.

78. R. Bhattacharyya and L. Frydman, *J. Chem. Phys.*, 2007, **127**, 194503.

79. K. J. Harris, A. Lupulescu, B. E. G. Lucier, L. Frydman, and R. W. Schurko, *J. Magn. Reson.*, 2012, **224**, 38.

80. D. Massiot, I. Farnan, N. Gautier, D. Trumeau, A. Trokiner, and J. P. Coutures, *Solid State Nucl. Magn. Reson.*, 1995, **4**, 241.

81. L. A. O'Dell and R. W. Schurko, *Chem. Phys. Lett.*, 2008, **464**, 97.

82. T. Kobayashi, F. A. Perras, T. W. Goh, T. L. Metz, W. Huang, and M. Pruski, *J. Phys. Chem. Lett.*, 2016, **7**, 2322.

83. T. Kobayashi, F. A. Perras, A. Murphy, Y. Yao, J. Catalano, S. A. Centeno, C. Dybowski, N. Zumbulyadis, and M. Pruski, *Dalton Trans.*, 2017, **46**, 3535.

84. D. A. Hirsh, A. J. Rossini, L. Emsley, and R. W. Schurko, *Phys. Chem. Chem. Phys.*, 2016, **18**, 25893.

85. K. R. Thurber and R. Tycko, *J. Chem. Phys.*, 2012, **137**, 084508.

86. D. J. Kubicki, A. J. Rossini, A. Purea, A. Zagdoun, O. Ouari, P. Tordo, F. Engelke, A. Lesage, and L. Emsley, *J. Am. Chem. Soc.*, 2014, **136**, 15711.

87. S. P. Brown, *Solid State Nucl. Magn. Reson.*, 2012, **41**, 1.

88. C. A. Fyfe, Y. Feng, H. Gies, H. Grondey, and G. T. Kokotailo, *J. Am. Chem. Soc.*, 1990, **112**, 3264.

89. D. H. Brouwer, R. J. Darton, R. E. Morris, and M. H. Levitt, *J. Am. Chem. Soc.*, 2005, **127**, 10365.

90. C. A. Fyfe, H. Grondey, Y. Feng, and G. T. Kokotailo, *J. Am. Chem. Soc.*, 1990, **112**, 8812.

91. A. J. Rossini, A. Zagdoun, F. Hegner, M. Schwarzwälder, D. Gajan, C. Copéret, A. Lesage, and L. Emsley, *J. Am. Chem. Soc.*, 2012, **134**, 16899.

92. H. Takahashi, D. Lee, L. Dubois, M. Bardet, S. Hediger, and G. De Paëpe, *Angew. Chem. Int. Ed.*, 2012, **51**, 11766.

93. A. J. Rossini, C. M. Widdifield, A. Zagdoun, M. Lelli, M. Schwarzwälder, C. Copéret, A. Lesage, and L. Emsley, *J. Am. Chem. Soc.*, 2014, **136**, 2324.

94. D. Lee, G. Monin, N. T. Duong, I. Z. Lopez, M. Bardet, V. Mareau, L. Gonon, and G. De Paëpe, *J. Am. Chem. Soc.*, 2014, **136**, 13781.

95. G. Mollica, M. Dekhil, F. Ziarelli, P. Thureau, and S. Viel, *Angew. Chem. Int. Ed.*, 2015, **54**, 6028.

96. Y. Matsuki, T. Idehara, J. Fukazawa, and T. Fujiwara, *J. Magn. Reson.*, 2016, **264**, 107.

97. T. Kobayashi, D. Singappuli-Arachchige, Z. Wang, I. I. Slowing, and M. Pruski, *Phys. Chem. Chem. Phys.*, 2017, **19**, 1781.

98. F. A. Perras, H. Luo, X. Zhang, N. S. Mosier, M. Pruski, and M. M. Abu-Omar, *J. Phys. Chem. A*, 2017, **121**, 623.

99. A. R. Mouat, T. Kobayashi, M. Pruski, T. J. Marks, and P. C. Stair, *J. Phys. Chem. C*, 2017, **121**, 6060.

100. T. Kobayashi, I. I. Slowing, and M. Pruski, *J. Phys. Chem. C*, 2017, **121**, 24687.

101. K. Märker, S. Paul, C. Fernández-de-Alba, D. Lee, J.-M. Mouesca, S. Hediger, and G. De Paepe, *Chem. Sci.*, 2017, **8**, 974.

102. M. Wilhelm, H. Feng, U. Tracht, and H. W. Spiess, *J. Magn. Reson.*, 1998, **134**, 255.

103. I. de Boer, L. Bosman, J. Raap, H. Oschkinat, and H. J. M. de Groot, *J. Magn. Reson.*, 2002, **157**, 286.

104. G. Tricot, J. Trebosc, F. Pourpoint, R. Gauvin, and L. Delevoye, *Ann. Rep. NMR Spectrosc.*, 2014, **81**, 145.

105. F. Pourpoint, A. S. L. Thankamony, C. Volkringer, T. Loiseau, J. Trébosc, F. Aussenac, D. Carnevale, G. Bodenhausen, H. Vezin, O. Lafon, and J.-P. Amoureux, *Chem. Commun.*, 2014, **50**, 933.

106. L. Piveteau, T.-C. Ong, A. J. Rossini, L. Emsley, C. Copéret, and M. V. Kovalenko, *J. Am. Chem. Soc.*, 2015, **137**, 13964.

107. Z. Wang, Y. Jiang, O. Lafon, J. Trébosc, K. D. Kim, C. Stampfl, A. Baiker, J.-P. Amoureux, and J. Huang, *Nat. Commun.*, 2016, **7**, 13820.

108. M. Valla, A. J. Rossini, M. Caillot, C. Chizallet, P. Raybaud, M. Digne, A. Chaumonnot, A. Lesage, L. Emsley, J. A. van Bokhoven, and C. Copéret, *J. Am. Chem. Soc.*, 2015, **137**, 10710.

109. A. G. M. Rankin, P. B. Webb, D. M. Dawson, J. Viger-Gravel, B. J. Walder, L. Emsley, and S. E. Ashbrook, *J. Phys. Chem. C*, 2017, **121**, 22977.

110. Z. Gan, *Chem. Commun.*, 2006, 4712.

111. F. A. Perras, J. D. Padmos, R. L. Johnson, L.-L. Wang, T. J. Schwartz, T. Kobayashi, J. H. Horton, J. A. Dumesic, B. H. Shanks, D. D. Johnson, and M. Pruski, *J. Am. Chem. Soc.*, 2017, **139**, 2702.

112. R. P. Sangodkar, B. J. Smith, D. Gajan, A. J. Rossini, L. R. Roberts, G. P. Funkhouser, A. Lesage, L. Emsley, and B. F. Chmelka, *J. Am. Chem. Soc.*, 2015, **137**, 8096.

113. T. Gullion and J. Schaefer, *J. Magn. Reson.*, 1989, **81**, 196.